

A Computer Vision Enabled damage detection model with improved YOLOv5 based on Transformer Prediction Head

Arunabha M. Roy¹ and Jayabrata Bhaduri²

¹*Aerospace Engineering Department, University of Michigan, Ann Arbor, MI 48109, USA*

²*Capacloud AI, Deep Learning & Data Science Division, Kolkata, WB 711103, India.*

Abstract

Objective. Computer vision-based up-to-date accurate damage classification and localization are of decisive importance for infrastructure monitoring, safety, and the serviceability of civil infrastructure. Current state-of-the-art deep learning (DL)-based damage detection models, however, often lack superior feature extraction capability in complex and noisy environments, limiting the development of accurate and reliable object distinction. *Method.* To this end, we present DenseSPH-YOLOv5, a real-time DL-based high-performance damage detection model where DenseNet blocks have been integrated with the backbone to improve in preserving and reusing critical feature information. Additionally, convolutional block attention modules (CBAM) have been implemented to improve attention performance mechanisms for strong and discriminating deep spatial feature extraction that results in superior detection under various challenging environments. Moreover, an additional feature fusion layers and a Swin-Transformer Prediction Head (SPH) have been added leveraging advanced self-attention mechanism for more efficient detection of multiscale object sizes and simultaneously reducing the computational complexity. *Results.* Evaluating the model performance in large-scale Road Damage Dataset

(RDD-2018), at a detection rate of 62.4 FPS, DenseSPH-YOLOv5 obtains a mean average precision (mAP) value of 85.25%, F1-score of 81.18%, and precision (P) value of 89.51% outperforming current state-of-the-art models. *Significance.* The present research provides an effective and efficient damage localization model addressing the shortcoming of existing DL-based damage detection models by providing highly accurate localized bounding box prediction. Current work constitutes a step towards an accurate and robust automated damage detection system in real-time in-field applications.

Keywords: Automated damage detection; You Only Look Once (YOLOv5) algorithm; Swin Transformer Object Detection (OD); Computer vision; Deep Learning (DL)

1. Introduction :

In recent years, automated damage detection plays an important role in various industrial applications including product quality assessment ([Agarwal and Singh, 2015](#); [Hanzaei et al., 2017](#)), infrastructure monitoring ([Eisenbach et al., 2017](#); [Gopalakrishnan, 2018](#)), safety and the serviceability of civil infrastructure ([Koch et al., 2015](#); [Hartmann and Trappey, 2020](#)). Early-stage accurate crack detection is critical for pavement damage rating and subsequent sealing or rehabilitation activities ([Chen et al., 2021](#); [Chen and Cho, 2022](#)). Therefore, it is important for roadway infrastructure engineers to detect pavement cracks accurately so that the best cost-effective plans of maintenance and rehabilitation could be employed ([Ni et al., 2022](#); [Dong et al., 2021](#)). While traditional damage detection techniques mainly include visual inspection, however, such labor-intensive methods have disadvantages due to their low efficiency, high cost, and individual biases ([Xu et al., 2022](#); [Shang et al., 2023](#)). Additionally, it is also limited in reproducibility, reliability, and objectivity due to the requirement of qualified personnel for domain-specific experience, knowledge, and skill sets ([Fang et al., 2020](#)). To circumvent such issues, more recently, various automatic and semi-automatic crack detection algorithms have gained significant attraction ([Gopalakrishnan, 2018](#)).

For the last three decades, image-based crack detection ([Mohan and Poobal, 2018](#); [Koch et al., 2015](#)) that include various image processing approaches, such as edge detection ([Zhao](#)

et al., 2010; Hanzaei et al., 2017; Li et al., 2022), dynamic thresholding (Oliveira and Correia, 2009; Wang et al., 2021b), and different morphological operations (Anitha et al., 2021; Li and Zhao, 2021) have been the central focus for detecting damage in challenging real-world scenarios. However, the aforementioned methods are quite sensitive to noise and varying illumination intensities, and hence, not suitable in real-world complex conditions (Koch et al., 2015). To circumvent such issues, later, conventional machine learning (ML) approaches have been introduced for damage detection (Mohan and Poobal, 2018; Koch et al., 2015). In general, such methods utilize a trained classifier such as a Support Vector Machine (SVM) on local feature descriptors that can be either Local Binary Patterns (LBP) (Varadharajan et al., 2014; Quintana et al., 2015) or Histogram of Oriented Gradient (HOG) (Kapela et al., 2015). Although, compared to conventional image processing approaches, ML-based models significantly improve the accuracy and efficiency of the damage detection, however, due to large errors in classification performances remains a serious bottleneck for deploying such models in real-world applications (Fang et al., 2020).

More recently, deep learning (DL) characterized by multilayer neural networks (NN) (LeCun et al., 2015) has shown remarkable breakthroughs in pattern recognition for various fields including image classification (Rawat and Wang, 2017; Jamil et al., 2022; Khan et al., 2022b,a), computer vision (Voulodimos et al., 2018; Roy and Bhaduri, 2021; Roy et al., 2022c; Roy and Bhaduri, 2022; Roy et al., 2022a), object detection (Zhao et al., 2019a; Chandio et al., 2022; Roy et al., 2022b; Singh et al., 2023a), brain-computer interfaces (Roy, 2022b,a,c; Singh et al., 2023b), signal classification (Jamil and Roy, 2023, 2022) and across diverse scientific disciplines (Bose and Roy, 2022; Roy and Bose, 2023b; Roy and Guha, 2022; Roy and Bose, 2023a; Roy and Guha, 2023). Following the success, there is an increasing thrust of research works geared towards damage classification tasks employing DL techniques, mostly convolutional neural networks (CNN), such as ResNet (Bang et al., 2018), AlexNet (Dorafshan et al., 2018; Li et al., 2018), VGG-net (Gopalakrishnan et al., 2017; Silva and Lucena, 2018) and various others (Chow et al., 2020; Nath et al., 2022; Li et al., 2021). Particularly in object localization, DL methods have demonstrated superior accuracy (Han et al., 2018) that can be categorized into two classes: two-stage and one-stage detector (Lin et al., 2017a). Two-stage detectors including Region Convolution Neural Network (R-CNN) (Girshick, 2015), faster R-CNN (Ren

et al., 2016), mask R-CNN (He et al., 2017) etc that have shown a significant improvement in accuracy in object localization. In recent times, You Only Look Once (YOLO) variants (Redmon et al., 2016; Redmon and Farhadi, 2017, 2018; Bochkovskiy et al., 2020) have been proposed that unify target classification and localization. In (Roy et al., 2022c; Roy and Bhaduri, 2022, 2021), DenseNet (Huang et al., 2017) blocks attaching Spatial Pyramid Pooling (SPP) (He et al., 2015) with an improved modified Path Aggregation Network (PANet) (Liu et al., 2018) has been integrated to enhance the representation of receptive fields and extraction of important contextual features in the original YOLOv4 leading to significant improvement in the detection speed and accuracy. In order to enhance gradient performance and reduce the computational cost, YOLOv4 (Bochkovskiy et al., 2020) designs a cross-stage partial (CSP) network. To further improve detection accuracy, YOLOv4 implements Mish activation (Misra, 2020) and CIoU loss (Zheng et al., 2020). Recently, Scaled-YOLOv4 (Wang et al., 2021a) demonstrated its superior performance in detecting the vast range of linearly scaled objects for various applications. As the latest generation of the YOLO series, the YOLOv5 (Jocher et al., 2021) has been rated top among state-of-the-art object detection models which inherit all the above advantages. Thus, in the present work, YOLOv5 has been considered a benchmark model for multiclass damage detection. More recently, improved YOLOv5 Based on Transformer Prediction Head (TPH-YOLOv5) (Zhu et al., 2021) has been proposed integrating convolutional block attention module (CBAM) (Woo et al., 2018) for closely packed object detection and Swin Transformer-enabled YOLOv5 (SPH-YOLOv5) (Gong et al., 2022) has been designed incorporating Normalization-based Attention Modules (NAM) that demonstrate significant improvement in accuracy while simultaneously reducing the computational complexity of the model which are the main motivations for the network architectural development of the current work.

1.1 Related Works :

In this section, some recent and relevant DL works have been highlighted in the field of road damage detection. In recent years, multiple studies have adopted various ML and DL-based approaches for automated road surface damage classification and detection (Zhang et al., 2017a;

(Stricker et al., 2019; Biçici and Zeybek, 2021) For instance, a smartphone-based supervised deep convolutional neural network (D-CNN) has been proposed for pavement damage classification (Zhang et al., 2016). Along a similar line, deep neural network (DNN) architecture has been employed for detecting cracks and potholes (Anand et al., 2018; Silva and Lucena, 2018) as well as pavement condition assessment (Fan et al., 2018). In Nhat-Duc et al. (2018), the superiority of the DCNN-based approach has been demonstrated over edge-detection-based approaches for pavement crack detection. In Maeda et al. (2018), a real-time road damage detection model based on SDD has been proposed that has been trained on a publicly available large-scale road damage dataset (RDD-2018) for eight different categories of road damages. Due to the popularity of the dataset, various attempts have been made, notably using YOLO (Alfarrarjeh et al., 2018), Faster R-CNN (Kluger et al., 2018), Faster R-CNN with ResNet-152 (Wang et al., 2018a), Ensemble models with Faster R-CNN and SSD (Wang et al., 2018b), and RetinaNet (Angulo et al., 2019) to further improve the detection performance. In addition, RetinaNet (Angulo et al., 2019) has been used on a modified RDD-2018 dataset which demonstrates significant performance improvement. Following the work of Maeda et al. (2018), progressive growing- generative adversarial networks (PG-GANs) (Maeda et al., 2021) with Poisson blending have been used to generate new training data (RDD-2019) in order to improve the accuracy of road damage detection. More recently, transfer learning (TL)-based road damage detection model (Arya et al., 2021a) has been proposed introducing large-scale open-source dataset RDD2020 (Arya et al., 2020, 2021b) considering multiple countries. In Naddaf-Sh et al. (2020), EfficientDet-D7 has been employed for the detection of asphalt pavement distress. Whereas, YOLO CSPDarknet53 (Mandal et al., 2020) has been used for road damage detection. Similarly, the YOLO network has been used for detecting pavement distress from high-resolution images (Du et al., 2021). In Majidifard et al. (2020), YOLOv2 model has been utilized for pavement distress classification from Google street view images. Along a similar line, a CNN-based predictive model trained in Google API images has been employed for detecting potholes in Patra et al. (2021). In a separate work in Guan et al. (2021), a stereo-vision integrated segmentation-based DL model with modified depth-wise separable convolution U-net has been deployed for crack and pothole detection where multi-feature image datasets have been used to train the model. More recently, a semi-supervised DL-based pixel-level segmentation

model (Karaaslan et al., 2021) has been proposed utilizing attention guidance for cracks and spalls localization that reduces computational cost significantly. In separate work, an improved YOLOv5 road damage detection algorithm (Guo and Zhang, 2022) has been proposed leveraging MobileNetV3 as a backbone feature extractor. In Hacıfendioğlu and Başağa (2022), Faster R-CNN has been employed for concrete pavement crack detection under various illumination and weather conditions. Although, there exist several state-of-the-art works for damage detection including multi-class damage localization models, however, they often suffer from low accuracy, missed detection, and relatively large computational overhead (Cao et al., 2020; Azimi et al., 2020; Naddaf-Sh et al., 2020).

1.2 Motivations :

Despite illustrating outstanding performance in damage detection, current state-of-the-art DL algorithms still require further improvement due to their insufficient fine-grain contextual feature extraction capability leading to missed detection and false object predictions for various damages/cracks which possess a wide range of textures, shapes, sizes, and colors (Cao et al., 2020; Azimi et al., 2020; Naddaf-Sh et al., 2020). Between various damage classes, accurate detection and localization tasks can be challenging due to significant variability of lightening conditions, low visibility, the coexistence of multi-object classes with various aspect ratios, and other morphological characteristics (Azimi et al., 2020; Naddaf-Sh et al., 2020). Additionally, visual similarities, complex backgrounds, and various other critical factors offer additional difficulties for the state-of-the-art damage detection models (Naddaf-Sh et al., 2020). To this end, the current works aim to develop an efficient and robust damage classification and accurate damage localization model simultaneously productive in terms of training time and computational cost which is currently lacking in the recent state-of-the-art endeavors.

1.3 Contributions :

To address the aforementioned shortcomings, in the current study, we present DenseSPH-YOLOv5 based on an improved version of the state-of-art YOLOv5 detection model for accurate real-time

damage detection. The major contributions of the present research work can be summarized as follows:

- In Dense-SPH-YOLOv5, we have attached DenseNet blocks with CSP modules in the CSPDarknet53 to preserve critical feature maps and efficiently reuse the discriminating feature information.
- Secondly, we have introduced an additional detection head specifically for detecting tiny objects in the head part of the proposed DenseSPH-YOLOv5 network.
- In addition, the convolutional block attention module (CBAM) has been implemented for the construction of progressive feature attention with large coverage along both channel and spatial dimensions for strong and discriminating deep spatial feature extraction during object detection.
- Furthermore, the regular CNN prediction heads (CPH) in YOLOv5 have been upgraded with Swin transformer Prediction Heads (SPHs) employing Swin transformer (STR) encoder block leveraging advanced self-attention mechanisms for efficient detection of multi-scale object sizes and simultaneously reducing the computational complexity.
- Spatial Pyramid Pooling (SPP) has been tightly attached to the backbone to enhance the representation of receptive fields and extraction of important contextual features.
- Finally, an improved modified Path Aggregation Network (PANet) has been utilized to efficiently preserve fine-grain localized information by feature fusion in a multi-scale feature pyramid map.

With the aforementioned modifications, the detection accuracy of the model has been significantly enhanced for multi-scale object detection. An extensive ablation study has been performed for different combinations of backbone-neck architecture in order to optimize both accuracies of detection and detection speed. The proposed DenseSPH-YOLOv5 has been employed to detect distinct eight different damage classes that provide superior and accurate detection under various complex and challenging environments. The present work effectively addresses the shortcoming of existing DL-based crack detection models and illustrates its

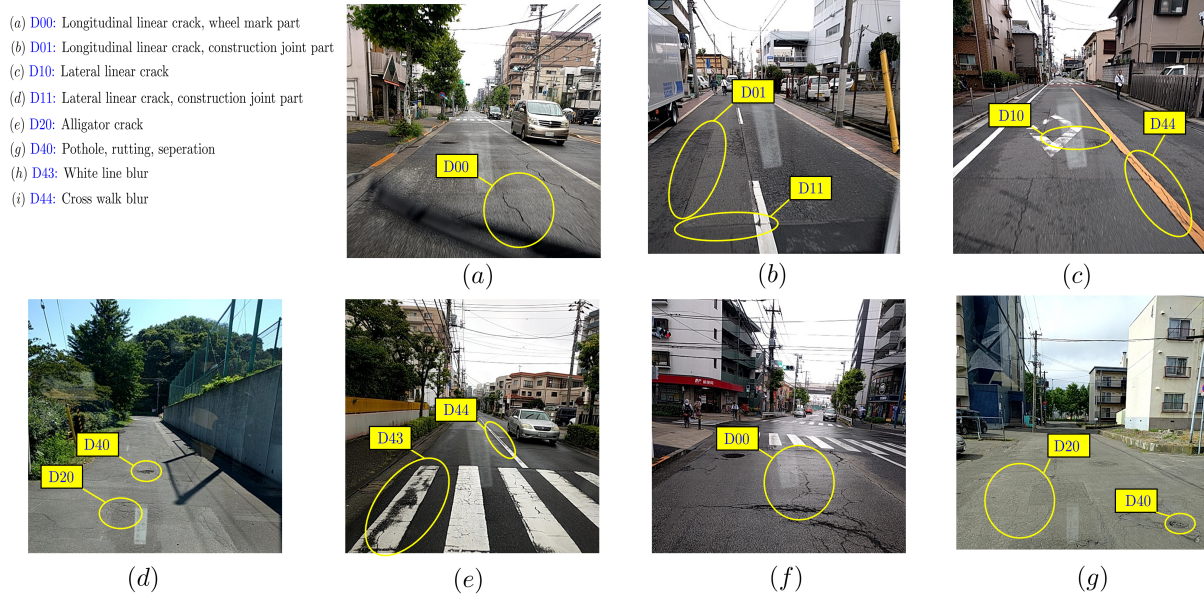


Figure 1: Sample images from RDD-2018 dataset (Maeda et al., 2018): (a) to (g) correspond to each of the eight categories with the legends.

superior potential in real-time in-field applications. The rest of the paper is organized as follows: description of the dataset has been described in Section 2; Section 3 introduces the proposed methodology for damage detection; the relevant finding and discussion of the proposed model have been discussed in Sections 4 and 5, respectively. Finally, the conclusions of the present work have been discussed in section 6.

2. Road Damage Dataset :

In the current study, large-scale Road Damage Dataset (RDD-2018) (Maeda et al., 2018) has been used that consists of 9,053 labeled road damage images of resolution 600×600 pixels containing a total number of 15,435 annotated bounding boxes for eight different types of road damage. To avoid biases, the images have been photographed in various weather and illumination conditions from different regions of Japan including Chiba, Muroran, Ichihara, Sumida, Nagakute, and Numazu. During annotation, professional road damage expertise has been employed to verify various damage classes that ensure the reliability of the dataset. Various damage types and corresponding class identifiers have been listed in Table. 1. Each

Table 1: Various road damage types and corresponding class identifiers in RDD-2018 dataset (Maeda et al., 2018).

Class Identifier	Damage type	Alignment	Details
D00	Linear Crack	Longitudinal	Wheel-marked part
D01	Linear Crack	Longitudinal	Construction joint part
D10	Linear Crack	Lateral	Equal interval
D11	Linear Crack	Lateral	Construction joint part
D20	Alligator Crack	-	Partial pavement, overall pavement
D40	Other Crack	-	Pothole, rutting, separation
D43	Other Crack	-	White line blur
D44	Other Crack	-	Cross walk blur

type of damages have been illustrated in Fig. 1. Primarily, the damage has been classified into cracks or different corruptions. Then, the cracks have been divided into linear and alligator cracks. Whereas, other corruptions include both potholes and rutting as well as other road damage classes such as blurring of white lines.

3. Proposed Methodology for damage detection:

In object detection, target object classification and localization are performed simultaneously where the target class has been categorized and separated from the background. The purpose of object localization is to locate objects by drawing bounding boxes (BBs) on input images containing the entire object. This is particularly useful for counting endangered species for accurate surveying. To this end, the main goal of the current work is to develop an efficient and robust damage classification and accurate damage localization model. In this regard, different variants of YOLO (Redmon et al., 2016; Redmon and Farhadi, 2017, 2018; Bochkovskiy et al., 2020) are some of the best high-precision one-stage object detection models. More recently,

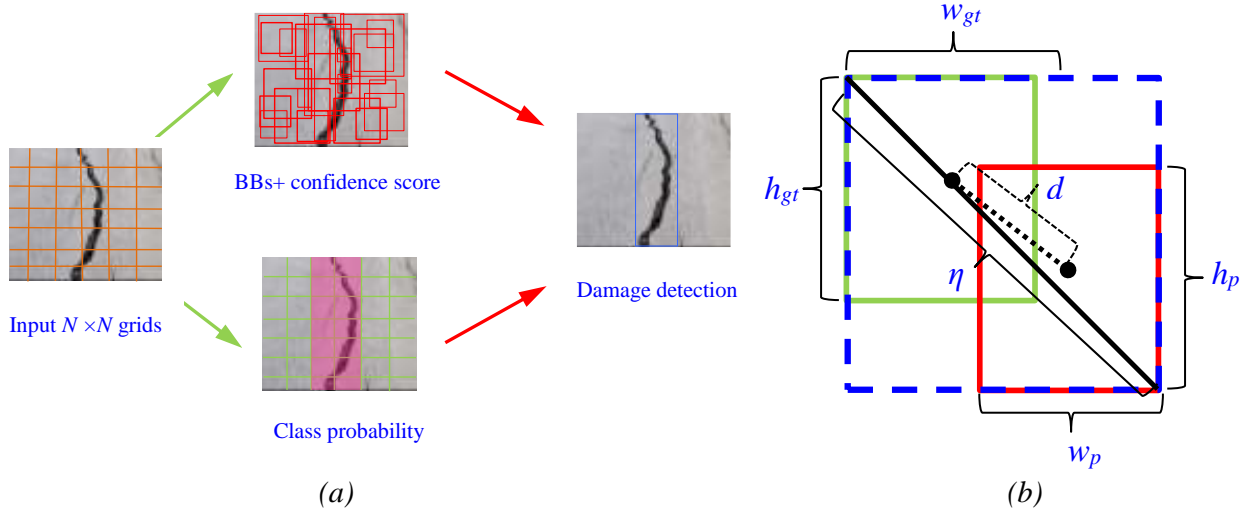


Figure 2: Schematic of (a) YOLO object localization process for damage localization; (b) Schematic of CIoU offset regression for target BBs predictions.

YOLOv5 (Jocher et al., 2021) has been introduced that currently achieves the best detection performance and has four different model variants including YOLOv5s, YOLOv5m, YOLOv5l, and YOLOv5x depend on different model widths and depths. In general, the overall architecture of YOLOv5 consists of the following parts: a backbone for deep feature extraction, followed by the neck for gathered semantic feature fusion, and finally head network for object classification and localization. The original version of YOLOv5 utilizes CSPDarknet53 (Wang et al., 2020; Bochkovskiy et al., 2020) with SPP and PANet (Liu et al., 2018) as backbone and neck, respectively. Whereas, YOLO detection head (Redmon et al., 2016) has been employed in the detection head. The YOLO model transforms the object detection task into a regression problem by generating BBs coordinates and probabilities for each class as shown in Fig. 2. During the process, the inputted image size has been uniformly divided into $N \times N$ grids where B predictive BBs have been generated. Subsequently, a confidence score has been assigned if the target object falls inside that particular grid. It detects the target object for a particular class when the center of the ground truth lies inside a specified grid. During detection, each grid predicts N_B numbers of BBs with the confidence value Φ_B as:

$$\Phi_B = \mathcal{P}_r(obj) \times \text{IoU}_p^t \quad \forall \mathcal{P}_r(obj) \in 0, 1 \quad (1)$$

where $\mathcal{P}_r(obj)$ infers the accuracy of BB prediction, i.e., $\mathcal{P}_r(obj) = 1$ indicates that the target class falls inside the grid, otherwise, $\mathcal{P}_r(obj) = 0$. The degree of overlap between ground truth and the predicted BB has been described by the scale-invariant evaluation metric intersection over union (IoU) which can be expressed as

$$\text{IoU} = \frac{\mathbf{B}_p \cap \mathbf{B}_{gt}}{\mathbf{B}_p \cup \mathbf{B}_{gt}} \quad (2)$$

where \mathbf{B}_{gt} and \mathbf{B}_p are the ground truth and predicted BBs, respectively.

3.1 Loss in BBs regression :

To further improve BBs regression and gradient disappearance, generalized IoU (GIoU) (Rezatofighi et al., 2019) and distance-IoU (DIoU) (Zheng et al., 2020) as been introduced considering aspect ratios and orientation of the overlapping BBs. More recently, complete IoU (CIoU) (Zheng et al., 2020) has been proposed for improved accuracy and faster convergence speed in BB prediction which can be expressed as

$$\mathcal{L}_{\text{CIoU}} = 1 + \beta\xi + \frac{\alpha^2(\mathbf{b}_p, \mathbf{b}_{gt})}{\eta^2} - \text{IoU} \quad (3)$$

$$\xi = \frac{4}{\pi^2} \left(\tan^{-1} \frac{w_{gt}}{h_{gt}} - \tan^{-1} \frac{w_p}{h_p} \right)^2; \quad \beta = \frac{\xi}{(1 - \text{IoU}) + \xi'} \quad (4)$$

where \mathbf{b}_{gt} and \mathbf{b}_p denotes the centroids of \mathbf{B}_{gt} and \mathbf{B}_p , respectively; ξ and β are the consistency and trade-off parameters, respectively. As shown in Fig. 3 -(b), η is the smallest diagonal length of $\mathbf{B}_p \cup \mathbf{B}_{gt}$; w_{gt} , w_p are widths and h_{gt} , h_p are heights of \mathbf{B}_{gt} and \mathbf{B}_p , respectively. With increasing w_p/h_p , we get $\xi \rightarrow 0$ from Eq. 4. Therefore, to optimize the influence of ξ on the CIoU, w_p/h_p can be properly chosen for the detection model. Finally, the best BB prediction can be obtained from the non-maximum suppression (NMS) (Ren et al., 2016) algorithm from various scales. In object detection in the YOLO framework, The total loss function Δ_l consist of BB coordinate prediction error Δ_{cor} , IoU error Δ_{IoU} , classification error term Δ_{cl} . The loss

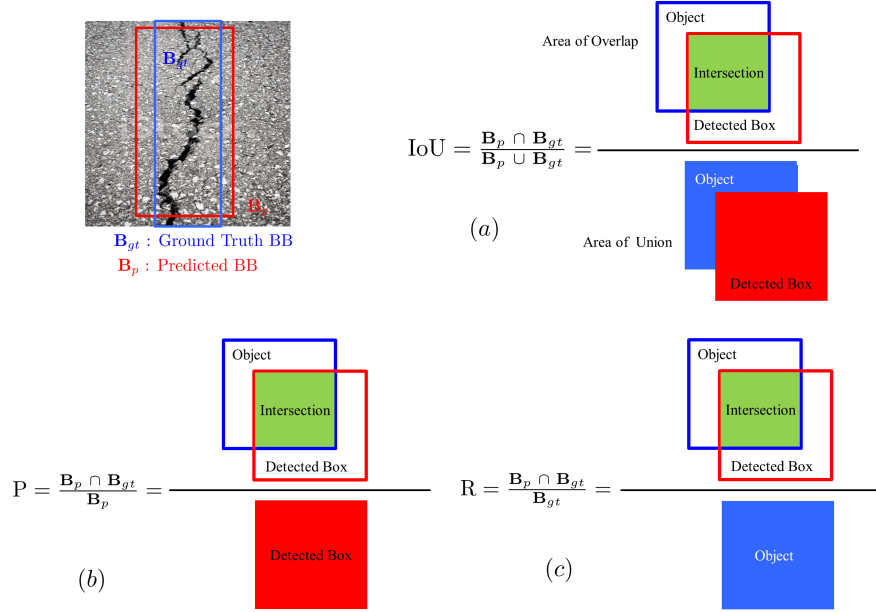


Figure 3: Schematic illustration of measuring various performance metrics: (a) Intersection over Union (IoU); (b) precision (P); (c) recall (R) during damage detection process.

function Δ_l for BBs regression can be formulated as,

$$\Delta_l = \Delta_{cor} + \Delta_{cl} + \Delta_{IoU}. \quad (5)$$

3.2 Performance metrics:

In the present work, the performance of the object detection models has been evaluated by common standard measures (Ferri et al., 2009) including average precision (AP), precision (P), recall (R), IoU, F-1 score, mean average precision (mAP), etc. The confusion matrix obtained from the evaluation procedure provides the following interpretations of the test results: true positive (TP), false positive (FP), false negative (FN), and true negative (TN). During object classification, the classified object can be defined as TP for $IoU \geq 0.5$. Whereas, it can be classified as FP for $IoU < 0.5$. Based on the aforementioned interpretations, the metric P of

the classifier can be defined by its ability to distinguish target classes correctly as :

$$P = \frac{TP}{(TP+FP)}; \quad (6)$$

The ratio of the correct prediction of target classes is called R of the classifier which can be evaluated as:

$$R = \frac{TP}{(TP+FN)} \quad (7)$$

The higher values of P and R indicate superior detection capability. Whereas, F-1 score is the arithmetic mean of the P and R given as :

$$F1 = 2 \times \left(\frac{P \ R}{P + R} \right) \quad (8)$$

A relatively high F1 score represents a robust detection model. The performance metrics AP can be defined as the area under a P-R curve ([Davis and Goadrich, 2006](#)) as follows

$$AP = \int_0^1 P(R) dR \quad (9)$$

A higher average AP value indicates better accuracy in predicting various object classes. In addition, $AP_{50:95}$ denotes AP over IoU=0.50 : 0.05 : 0.95; AP_{50} and AP_{75} are APs at IoU threshold of 50% and 75%, respectively. The AP for detecting small, medium, and large objects can be measured through AP_S , AP_M , and AP_L , respectively. Finally, mAP can be obtained from the average of all APs as:

$$mAP = \frac{1}{N_c} \sum_{i=1}^N AP_i. \quad (10)$$

In YOLOv5, various combinations of activation functions including sigmoid, leaky- ReLU and SiLU ([Hendrycks and Gimpel, 2016](#)) can be utilized to improve the performance of the model for a specific detection task. In addition, bag of freebies and specials ([Bochkovskiy et al., 2020](#)) can also be employed to further optimize the detection architecture of YOLOv5. As the latest generation of the YOLO series, YOLOv5 has been shown to provide state-of-the-art detection performance. Therefore, it has been chosen as the baseline model for our present study.

3.3 DenseSPH-YOLOv5 architecture:

In recent years, various attempts have been made on DL-based computer vision models for damage detection such as Faster R-CNN (Kluger et al., 2018; Wang et al., 2018a), SSD (Maeda et al., 2018; Wang et al., 2018b), RetinaNet (Angulo et al., 2019), YOLO (Alfarrarjeh et al., 2018; Mandal et al., 2020), YOLOv2 (Majidifard et al., 2020), YOLOv5 (Guo and Zhang, 2022) etc. Although the aforementioned techniques have demonstrated outstanding performance, however, the damage detection task faces several challenges, in particular, due to the presence of complex and noisy backgrounds, significant variability of lightening conditions, low visibility, densely packed classes, and overlap, the coexistence of multi-object classes with various aspect ratios, and other morphological characteristics (Azimi et al., 2020; Naddaf-Sh et al., 2020). In this regard, YOLOv5 can be a suitable model which demonstrates both superior accuracy and faster detection speed compared to YOLOv4. The state-of-the-art YOLOv5 is comparatively light, yet effective, which performs multiple downsampling and turns shallow semantic information into high-level semantic information that effectively reduces the number of parameters. However, this inevitably loses semantic information and makes the network ineffective at extracting and fusing discriminating semantic features. Therefore, the original YOLOv5 network requires further improvement due to its insufficient fine-grain contextual feature extraction capability leading to missed detection and false object predictions for various damages/cracks which possess a wide range of textures, shapes, sizes, and colors (Cao et al., 2020; Azimi et al., 2020; Naddaf-Sh et al., 2020). In order to achieve high accuracy and high efficiency in damage detection, we propose a novel object localization algorithm DenseSPH-YOLOv5 based on a state-of-the-art YOLOv5 network to enhance feature extraction, preserve fine-grain localized information and improve feature fusion that provides superior damage detection under various challenging environments. The overall network of the DenseSPH-YOLOv5 model is shown in Fig. 4. To improve performance in terms of classification accuracy and object localization, we perform extensive experiments, and various modifications are proposed which are detailed in the subsequent sections.

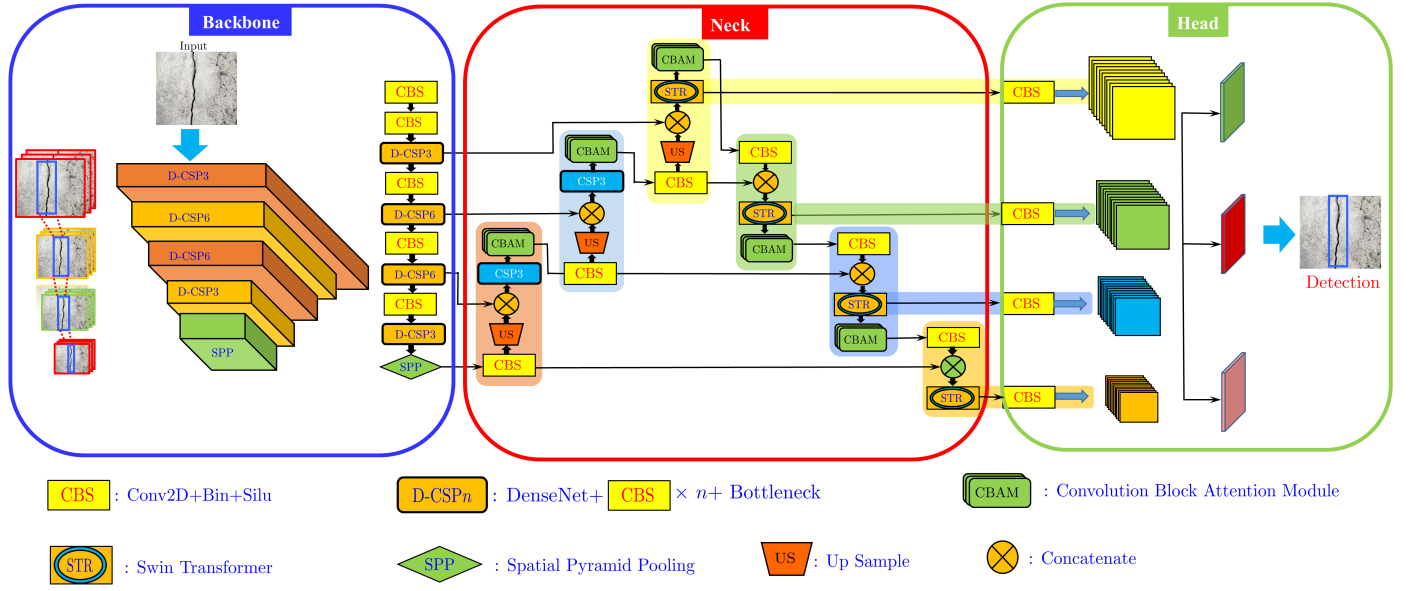


Figure 4: Schematic of the proposed DenseSPH YOLOv5 with fused DenseNet in CSPDarknet53 backbone; CBAM module in the improved neck; four SPHs utilize hierarchical feature maps from STR encoder blocks in the modified Neck.

3.3.1 DenseNet block : Since YOLOv5 reduces the feature maps from the inputted images through convolution and down-sampling procedures that result in significant semantic feature loss during transmission. To this end, we have introduced DenseNet (Huang et al., 2017) in the original CSPDarknet53 of YOLOv5 attached to the CSP module to preserve critical feature maps and efficiently reuse the discriminative feature information as shown in Fig. 4. In DenseNet, each layer has been connected to other layers in a feed-forward mode where n -th layer can receive the important feature information ξ_n from all the previous layers $\xi_0, \xi_1, \dots, \xi_{n-1}$ as:

$$\xi_n = \Theta_n[\xi_0, \xi_1, \dots, \xi_{n-1}] \quad (11)$$

where Θ_n is the feature map function for n -th layer. The schematic of the DenseNet blocks network structure have been shown in Fig. 5-(d). Through our extensive experiments, we found out that DenseNet improves the feature transfer and mitigates over-fitting in the detection network. Therefore, in the proposed Dense-SPH YOLOv5 network, as shown in Fig. 3, we have introduced four DenseNet blocks: the first block (Dense B-1) has been attached before cross-stage partial block CSP3; the second block (Dense B-2) has been placed before CSP6;

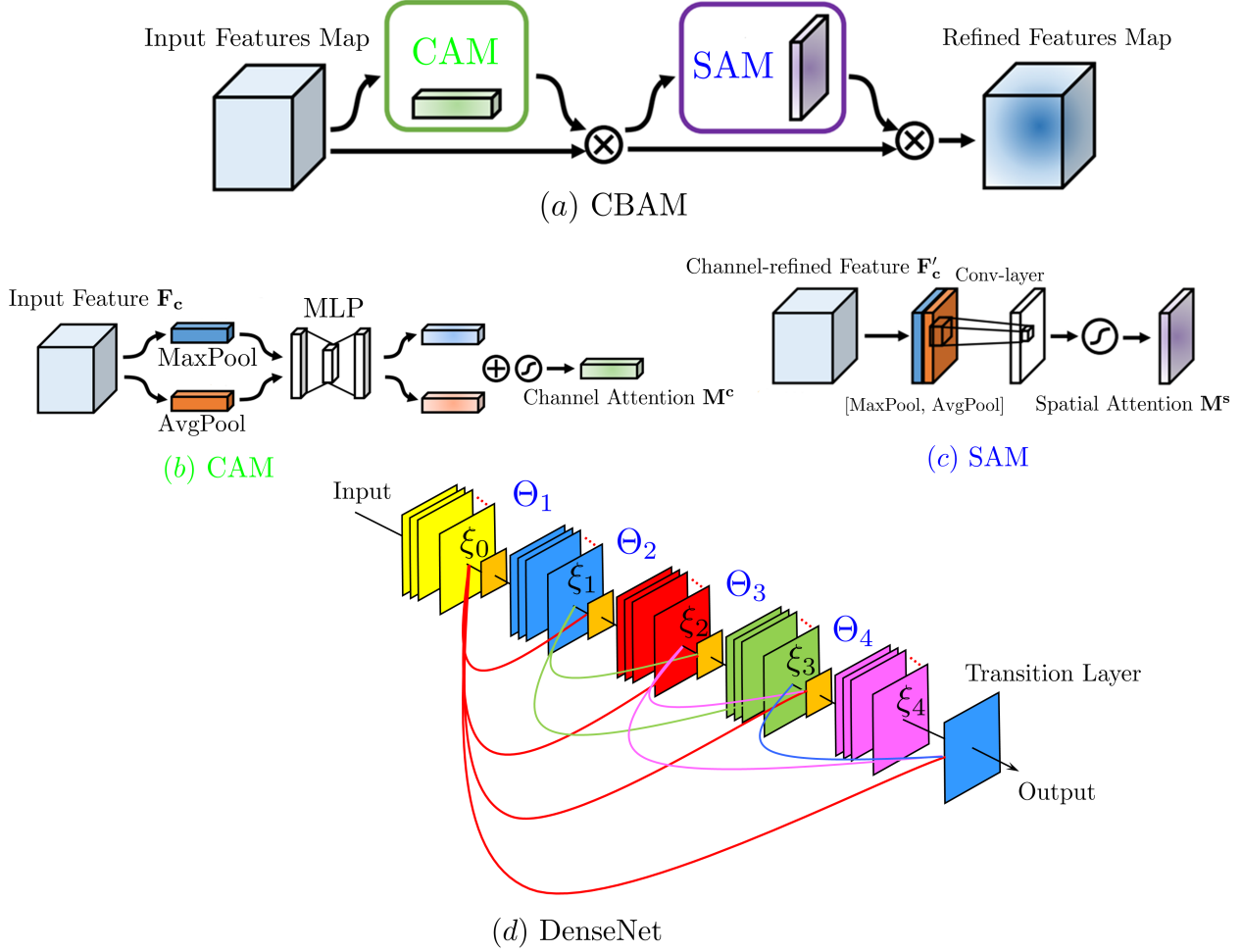


Figure 5: Schematic of (a) CBAM that has two sequential sub-modules: (b) CAM and (c) SAM for adaptive refinement of feature map at every intermediate convolution blocks; (d) network architecture of DenseNet block used in Dense-SPH YOLOv5 detection model.

whereas, third (Dense B-3) and fourth (Dense B-4) blocks have been added before CSP6 and CSP3, respectively which results in enhanced feature propagation. Additionally, by reducing redundant feature operations, the Dense-CSPDarknet53 network improves the computational speed.

3.3.2 Convolutional block attention module (CBAM): Convolutional block attention module (CBAM) (Woo et al., 2018) is a lightweight, yet effective attention block which can be integrated into the object detection model in an end-to-end manner that has shown superior detection accuracy (Zhu et al., 2021). For an inputted feature map, CBAM sequentially employs the attention map along the channel and spatial dimensions. As shown in Fig. 5-(a), the network structure of the CBAM module consists of two sequential sub-modules: Channel Attention Module (CAM) and Spatial Attention Module (SAM) for adaptive refinement of the feature map at every intermediate convolution blocks by multiplying input feature map with the attention map. For inputted feature map $\mathbf{F}_c \in \mathbb{R}^{C \times H \times W}$, CAM produces 1D channel attention map $\mathbf{M}^c \in \mathbb{R}^{C \times 1 \times 1}$, and sequentially, SAM infers 2D spatial attention map $\mathbf{M}^s \in \mathbb{R}^{1 \times H \times W}$ as shown in Figs. 4-(a-c). The overall CBAM attention process can be expressed as:

$$\mathbf{F}'_c = \mathbf{M}^c(\mathbf{F}_c) \otimes \mathbf{F}_c; \quad \mathbf{F}''_c = \mathbf{M}^s(\mathbf{F}'_c) \otimes \mathbf{F}'_c; \quad (12)$$

where ; \mathbf{F}''_c is the CBAM refined output; \otimes represents element-wise multiplication. More specifically, CAM produces two different spatial descriptors including average-pooled features \mathbf{F}_{avg}^c and max pooled features \mathbf{F}_{max}^c which produce channel attention map $\mathbf{M}^c \in \mathbb{R}^{C \times 1 \times 1}$ from multi-layer perceptron (MLP). The CAM attention can be expressed as:

$$\mathbf{M}^c(\mathbf{F}_c) = \sigma(\mathbf{W}_1(\mathbf{W}_0(\mathbf{F}_{avg}^c))) + \mathbf{W}_1(\mathbf{W}_0(\mathbf{F}_{max}^c)) \quad (13)$$

where $\mathbf{W}_0 \in \mathbb{R}^{C/r \times C}$, and $\mathbf{W}_1 \in \mathbb{R}^{C \times C/r}$ are the MLP weights ; σ represents the sigmoid activation function. In SAM, inter-spatial attention map $\mathbf{M}^s(\mathbf{F}_c) \in \mathbb{R}^{H \times W}$ has been aggregated to generate 2D maps: $\mathbf{F}_{avg}^s \in \mathbb{R}^{1 \times H \times W}$ and $\mathbf{F}_{max}^s \in \mathbb{R}^{1 \times H \times W}$. From these two feature maps, the

spatial attention can be computed as:

$$\mathbf{M}_s(\mathbf{F}) = \sigma(f^{n \times n}([\mathbf{F}_{avg}^s; \mathbf{F}_{max}^s])) \quad (14)$$

where $f^{n \times n}$ denotes a convolution operation with the filter size of $n \times n$ with $n = 7$. The implementation of the CBAM module into the proposed DenseSPH-YOLOv5 significantly improves the detection accuracy of the damage detection by providing specific attention to the dense objects and confusing noisy areas which proved the effectiveness of this module. Overall, it helps to learn more expressive features that demonstrate significant improvement in detection accuracy for road damage datasets considered herein.

3.3.3 Swin transformer encoder blocks: Inspired by the superior performance of the vision transformer (Dosovitskiy et al., 2020) in dense and occluded object detection, in the proposed model, Swin transformer (STR) encoder blocks (Liu et al., 2021) have been fused to all four detection heads of DenseSPH-YOLOv5 architecture as shown in Fig. 3. Such implementation improves the global semantic feature extraction and contextual information fusion leveraging self-attention mechanism (Vaswani et al., 2017) that demonstrated superior performance in dense object detection (Gong et al., 2022).

For inputted feature map $\mathbf{F}_s \in \mathbb{R}^{H \times W \times C}$, it transforms to $\mathbf{Q}^s, \mathbf{K}^s, \mathbf{V}^s \in \mathbb{R}^{N \times C'}$ where $N = H \times W$ to feed Multi-head Self Attention (MSA) module after linear projection and reshape operations. The output feature map \mathbf{Z}^s from MSA aggregates global information which can be expressed as

$$\mathbf{Z}^s = \mathbf{A}^s \mathbf{V}^s; \quad \mathbf{A}^s = \text{softmax } \mathbf{Q}^s \mathbf{K}^{sT}; \quad (15)$$

where $\mathbf{A}^s \in \mathbb{R}^{N \times N}$ is the self-attention matrix that represents the relationship between feature map elements with remaining elements. Although, MSA in Transformer is effective in generating a self-attention matrix by integrating multiple independent subspaces, however, the global computation overhead is significantly high for high-resolution images. Thus, for dense prediction or to tackle high-resolution images, the computational complexity of MSA in Transformer is not suitable which leads to quadratic complexity with respect to the number of tokens

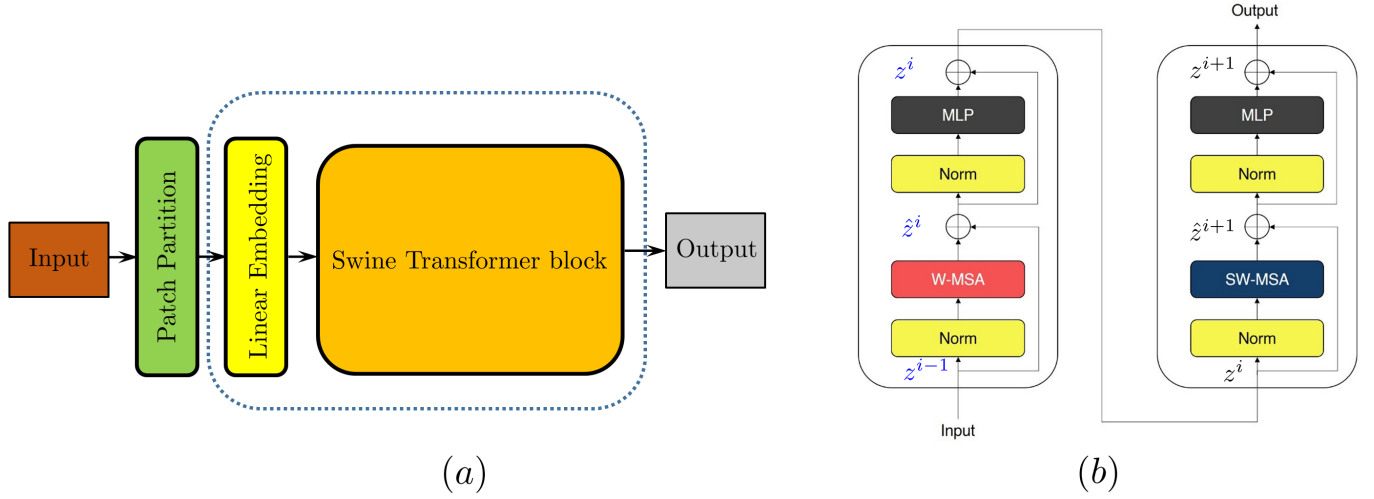


Figure 6: Schematic of (a) STR encoder architecture that contains (b) regular W-MSA and SW-MSA used in detection heads of DenseSPH-YOLOv5 architecture.

(Liu et al., 2021). To this end, STR can significantly improve the computational efficiency of MSA that has linear computational complexity with respect to image size which enhances the performance of the model in terms of detection speed and accuracy. Therefore, in the proposed DenseSPH-YOLOv5 detection model, the STR encoder module has been fused into four different prediction heads. As shown in Fig. 6 -(b), each STR encoder contains two sub-layers that include shifted window-based multi-head self-attention (MSA) module, followed by a fully-connected MLP with GeLU nonlinearity. Residual connections are used after each MSA module. Subsequently, Layer Norm (LN) has been added before MSA and MLP. In STR, the obtained feature map has been divided into non-overlapping separate windows in the W-MSA module. Subsequently, self-attention has been computed in each local window. Applying SW-MSA partitioning, the consecutive STR blocks can be computed as:

$$\hat{z}^i = \mathbf{W}\text{-MSA}(\mathbf{LN}(z^{i-1})) + z^{i-1}; \quad z^i = \mathbf{MLP}(\mathbf{LN}(\hat{z}^i)) + \hat{z}^i \quad (16)$$

$$\hat{z}^{i+1} = \mathbf{SW}\text{-MSA}(\mathbf{LN}(z^i)) + z^i; \quad z^{i+1} = \mathbf{MLP}(\mathbf{LN}(\hat{z}^{i+1})) + \hat{z}^{i+1} \quad (17)$$

where z^i and \hat{z}^i represent the output features from MLP and SW-MSA modules, respectively. For a feature map $F_s \in \mathbb{R}^{H \times W \times C}$ with $m \times m$ size of local window, the computational complexity

Υ can be obtained as

$$\Upsilon(\mathbf{MSA}) = 4HWC^2 + 2(HW)^2C; \quad \Upsilon(\mathbf{W-MSA}) = 4HWC^2 + 2(HW)M^2C \quad (18)$$

where HW is the patch number. Evidently, for large HW , the computational overhead of global MSA is exceptionally high, while, W-MSA is scalable. Thus, implementing STR significantly reduces the computational complexity of the model.

3.3.4 Receptive field enhancement: One of the requirements of CNN is to have fixed-size input images. However, due to the different aspect ratios of the images, they have been fixed by cropping and warping during the convolution process which results in losing important features. In this regard, SPP (He et al., 2015) applies an efficient strategy in detecting target objects at multiple length scales. To this end, we have added an SPP block integrated with DCSP-3 in the Dense-CSPDarknet53 backbone to improve receptive field representation and extraction of important contextual features as shown in Fig. 4.

4. Results:

In this section, the performance and detection accuracy of the proposed DenseSPH-YOLOv5 framework have been discussed that been evaluated in the RDD-2018 dataset consisting of 8 different categories of damage classes. For better clarity in BB representation, each damage type has been marked with the corresponding class identifiers as shown in Table 1. The performance of the DenseSPH-YOLOv5 network has been optimized through extensive ablation studies. Finally, the performance of the proposed model has been studied in detail and compared with several state-of-the-art object detection models.

4.1 Training procedure :

In the present work, we have performed an extensive and elaborate study to explore the comparative performance analysis of the proposed DenseSPH-YOLOv5 models for road damage localization tasks. From the RDD-2018 dataset, a total of 80% and 20% images have been

randomly chosen for training and validation, respectively. For all the experiments, we have used a Windows 10 Pro (64-bit) based computational system that has Intel Core i5-10210U with CPU @ 2.8 GHz $\times 6$, 32 GB DDR4 memory, NVIDIA GeForce RTX 2080 utilizing GPU parallelization. As part of data augmentation, along with traditional methods such as photometric distortion and geometric distortions, additional data augmentation strategies including MixUp (Zhang et al., 2017b), CutMix (Yun et al., 2019) and Mosaic (Bochkovskiy et al., 2020) have been combined which help improves the performance of DenseSPH-YOLOv5. In addition, Mosaic augmentation can significantly enrich the background information. Since such a method increases the batch size, therefor, batch normalization has been followed. Unless otherwise stated, a batch size set to 16 with a total number of training steps has been kept as 80. The initial learning rate has been set to 0.01 with SGD optimizer. The training dataset has been trained to utilize the available pre-trained weights-file (Lin et al., 2014).

4.2 Optimization of network performance:

At first, we conduct extensive experiments to select proper backbone-neck combination modules to optimize the performance of the proposed DenseSPH-YOLOv5 model in terms of both detection accuracy and speed. For different combinations of backbone-neck configurations, detection accuracy in terms of parameters AP, AP₅₀, AP₇₅, AP_S, AP_M, and AP_L as well as detection speed (in FPS) has been reported in Table. 2. From the Table. 2, one can see the introducing Additional Detection Head (ADH) improves performance by employing an additional feature fusion mechanism. Notably, there are 2.3% increases in AP₅₀; and 6.1% increases in AP_L compared to the baseline original YOLOv5. Furthermore, implementation of DenseNet with ADH enhances the performance further, in particular, for relatively small object detection with 3.6 % increase in AP_L as shown in Fig. 7-(a). However, this results in a signification reduction in detection speed (from 69.1 FPS to 55.2 FPS). With the introduction of the CBAM in the neck part of the detection model, the detection performance improves further compared to DensNet+ADH configuration for relatively medium and large object sizes with 3.7% and 3.6% increase in AP_M and AP_L, respectively while slightly compromising the detection speed. Thus, the implementation of CBAM has been proven to be an effective

Table 2: Performance of various residual and dense block combinations in DenseSPH-YOLOv5 architecture for anchors size of 416×416 .

Backbone add-in	Neck add-in	AP	AP_{50}	AP_{75}	AP_S	AP_M	AP_L	FPS
(YOLOv5) -	-	69.2	71.7	83.2	61.2	78.3	81.4	70.2
-	ADH	70.4	74.1	85.9	67.3	79.7	84.7	69.1
DenseNet	ADH	74.5	79.7	88.5	70.9	81.2	85.1	55.2
DenseNet	ADH+CBAM	79.1	83.6	90.2	75.1	84.9	88.7	56.4
DenseNet	ADH+CBAM+STR	81.4	85.2	91.4	78.2	86.5	89.5	62.4

strategy to retain semantic and delicate spatial information from spatial and channel attention mechanisms that enhance the overall performance of the model. Finally, the best performance has been achieved when both CBAM and STR respectively have been integrated into the neck and detection head which demonstrate significant improvements in the accuracy parameter, in particular, AP , AP_{50} , AP_{75} , AP_M and AP_L increase by 12.2%, 13.5%, 8.2%, 8.3%, and 8.1%, respectively compared to original YOLOv5 configuration. Moreover, we have also observed improvement in detection speed with the introduction of STR in the detection head by reducing the computational complexity compared to only ADH+CBAM configuration in the neck as shown in Fig. 7-(a). Therefore, a such configuration in DenseSPH-YOLOv5 provides the optimal performance in terms of detection accuracy and speed for the road-damaged data set considered herein. In summary, together with proper activation function and improved backbone-neck combination in DenseSPH-YOLOv5 provides an efficient high-performance model for damage detection in complex scenarios.

4.3 State-of-the-art comparison:

In this section, the detection performance of the proposed DenseSPH-YOLOv5 has been compared with some of the existing state-of-the-art detection models (Zhao et al., 2019b). For the performance comparison, we have considered Faster R-CNN (Ren et al., 2016), RetinaNet (Lin et al., 2017b), SSD (Liu et al., 2016), YOLOv4 (Bochkovskiy et al., 2020), Dense-YOLOv4

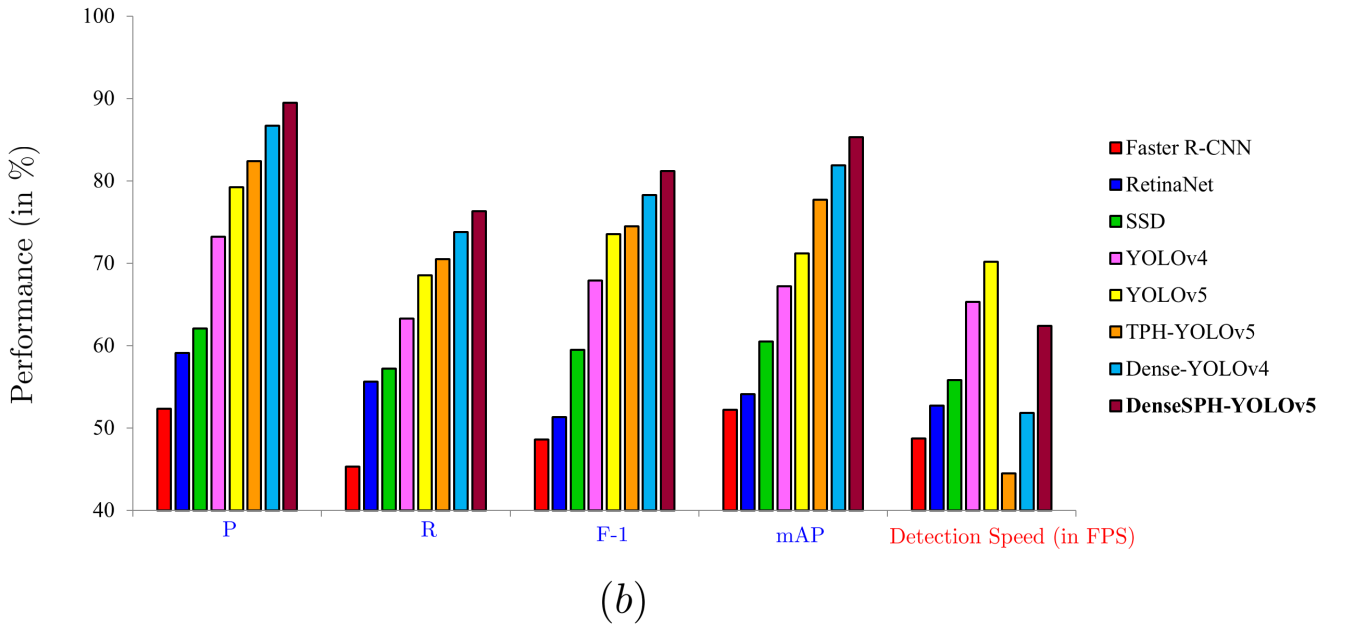
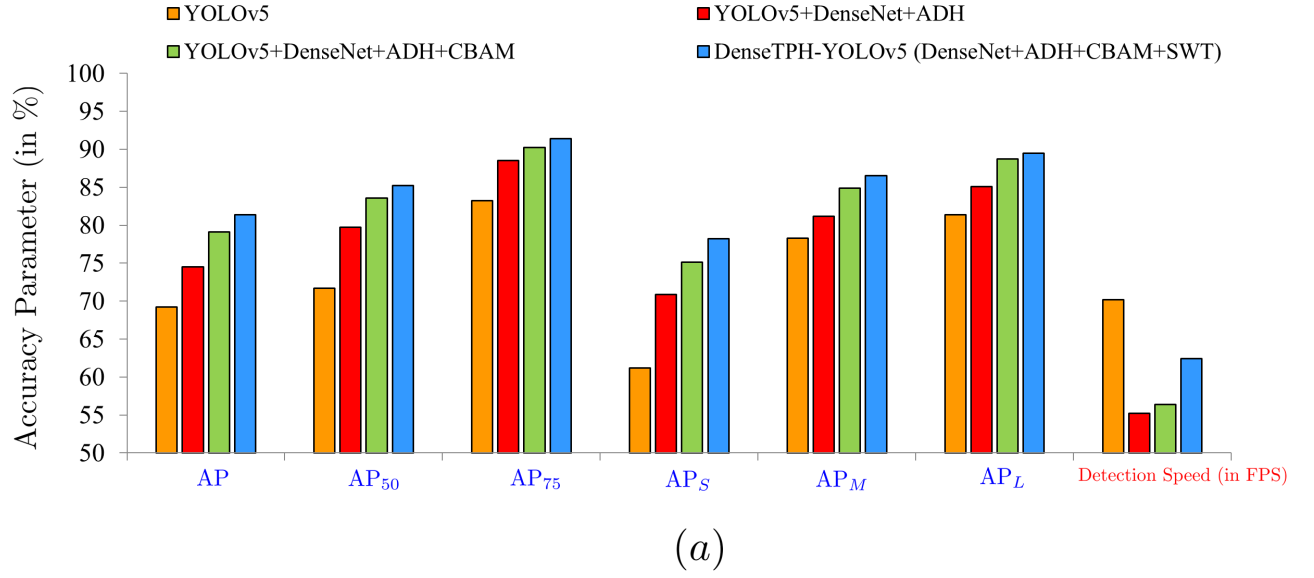


Figure 7: Comparison bar chart of precision parameters and detection speed for (a) different combinations of backbone and neck of the detection model; (b) different state-of-the-art models and DenseSPH-YOLOv5.

Table 3: Comparison of different performance parameters including P, R, F1, mAP, and detection speed (in FPS) between DenseSPH-YOLOv5 and other SOAT models where bold highlights the best performance values.

Model	P (%)	R (%)	F1-score (%)	mAP (%)	Dect. time (ms)	FPS
Faster R-CNN	52.32	45.39	48.60	52.17	20.50	48.7
RetinaNet	59.11	55.67	51.35	54.11	18.87	52.7
SSD	62.13	57.19	59.56	60.52	17.92	55.8
YOLOv4	73.22	63.35	67.93	67.13	15.31	65.3
YOLOv5	79.17	68.47	73.43	71.13	14.24	70.2
TPH-YOLOv5	82.37	70.51	74.52	77.62	22.47	44.5
Dense-YOLOv4	86.75	73.75	78.28	81.87	19.30	51.8
DenseSPH-YOLOv5	89.51	76.25	81.18	85.25	16.02	62.4

(Roy and Bhaduri, 2022), YOLOv5 (Jocher et al., 2021), and TPH-YOLOv5 (Zhu et al., 2021) that are trained in RDD-2018 dataset. Comparison of different performance parameters including P, R, F1-score, mAP, and detection speed obtained from these models have been presented in Table 3. The comparison reveals that the accuracy values obtained from Faster R-CNN, RetinaNet, and SSD are quite inferior compared to YOLO variants as visually illustrated in the bar-chart plot in Fig. 7-(b). Between YOLOv4 and YOLOv5, YOLOv5 demonstrated better performance with a 5.95% increase in P and 4.01% increase in mAP, respectively. We observe that the performance of Dense-YOLOv4 is superior to the TPH-YOLOv5 with 4.38%, 3.24%, 3.76%, and 4.25% increase in P, R, F1, and mAP, respectively. However, the proposed DenseSPH-YOLOv5 yields the best performance reaching the values of 89.51%, 76.25%, 81.18%, and 85.25% in P, R, F1, and mAP, respectively as shown in Fig. 7- (b). Moreover, DenseSPH-YOLOv5 provides a superior real-time detection speed of 62.4 FPS which is 28.68% and 16.98% higher than TPH-YOLOv5 and Dense-YOLOv4 models, respectively. In summary, DenseSPH-YOLOv5 outshines some of the best detection models in terms of both detection accuracy and speed illustrating its suitability for automated high-performance damage detection models.

4.4 Comparison with existing state-of-the-art damage detection models:

In addition, the performance of the DenseSPH-YOLOv5 has been compared with several existing state-of-the-art road damage detection models evaluated in RDD-2018 datasets. As shown in Table 4, we compared the performance from various DL models including SSD Inception v2 (Maeda et al., 2018), SSD MobileNet (Maeda et al., 2018), YOLO (Alfarrarjeh et al., 2018), Faster R-CNN (Kluger et al., 2018), Faster R-CNN with ResNet-152 (Wang et al., 2018a), Ensemble models with Faster R-CNN and SSD (Wang et al., 2018b), and RetinaNet (Angulo et al., 2019) with our Dense-YOLOv4 and DenseSPH-YOLOv5 models. Note, in (Angulo et al., 2019) additional images were included in the RDD-2018 dataset to improve the detection performance. From the direct comparison, two current state-of-the-art models Faster R-CNN with ResNet-152 (Wang et al., 2018a) and Ensemble models (Wang et al., 2018b) have reached the F1 value of 62.55% that is 2.63% improvement over SSD MobileNet (Maeda et al., 2018). While RetinaNet (Angulo et al., 2019) illustrated significant performance improvement, Dense-YOLOv4 performs better with F1 of 78.28% in the original RDD-2018 dataset. Relative to the aforementioned models, our proposed model has achieved the best F1 value of 81.18 % among current state-of-the-art damage detection models. In terms of other precision metrics, there are 3.64% and 10.51% improvements in P and R compared to RetinaNet (Angulo et al., 2019), respectively. Comparing detection speed, DenseSPH-YOLOv5 provides competitive performance compared to SSD Inception v2 (Maeda et al., 2018) elucidates its superiority in real-time damage detection.

4.5 Overall performance of DenseSPH-YOLOv5:

From section 4.3, we observed that TPH-YOLOv5, Dense-YOLOv4, and DenseSPH-YOLOv5 provide better performance compared to other SOAT models. Therefore, these three models are closely compared in terms of mAP, F1, IoU, final loss, and average detection time as shown in Table 5. The proposed DenseSPH-YOLOv5 has achieved the highest average IoU value of 0.803 indicating superior BB accuracy during target detection compared to the other two models. Similarly, it has also illustrated better detection performance and accuracy by achieving the

Table 4: Comparison of different performance parameters between DenseSPH-YOLOv5 and other SOAT road damage detection models evaluated in RDD-2018 dataset where bold highlights the best performance values.

Reference	Method	Performance	Det. Speed (FPS)
Maeda et al. (2018)	SSD Inception v2	F-1: 52.61; P: 81.10; R: 38.97	63.1
Maeda et al. (2018)	SSD MobileNet	F-1: 59.92; P: 81.11; R: 47.52	30.6
Alfarrarjeh et al. (2018)	YOLO	F-1: 62.00; P: -; R: -	-
Kluger et al. (2018)	Faster R-CNN	F-1: 61.00; P: -; R: -	-
Wang et al. (2018a)	Faster R-CNN (ResNet-152)	F-1: 62.55; P: -; R: -	-
Wang et al. (2018b)	Ensemble (Faster R-CNN+ SSD)	F-1: 62.55; P: -; R: -	-
Angulo et al. (2019)*	RetinaNet	F-1: 74.97; P: 85.87; R: 65.75	-
(Roy and Bhaduri, 2022)	Dense-YOLOv4	F-1: 78.28; P: 86.75; R: 73.75	51.8
Ours (current study)	DenseSPH-YOLOv5	F-1: 81.18; P: 89.51; R: 76.25	62.4

Table 5: Overall performance comparison between TPH-YOLOv5, Dense-YOLOv4, and DenseSPH-YOLOv5.

Detection model	IoU	F1	mAP	Validation loss	Detection time (ms)	Detection speed (FPS)
TPH-YOLOv5	0.740	0.745	0.776	18.07	22.47	44.5
Dense-YOLOv4	0.781	0.782	0.819	10.13	19.30	51.8
DenseSPH-YOLOv5	0.803	0.811	0.852	7.18	16.02	62.4

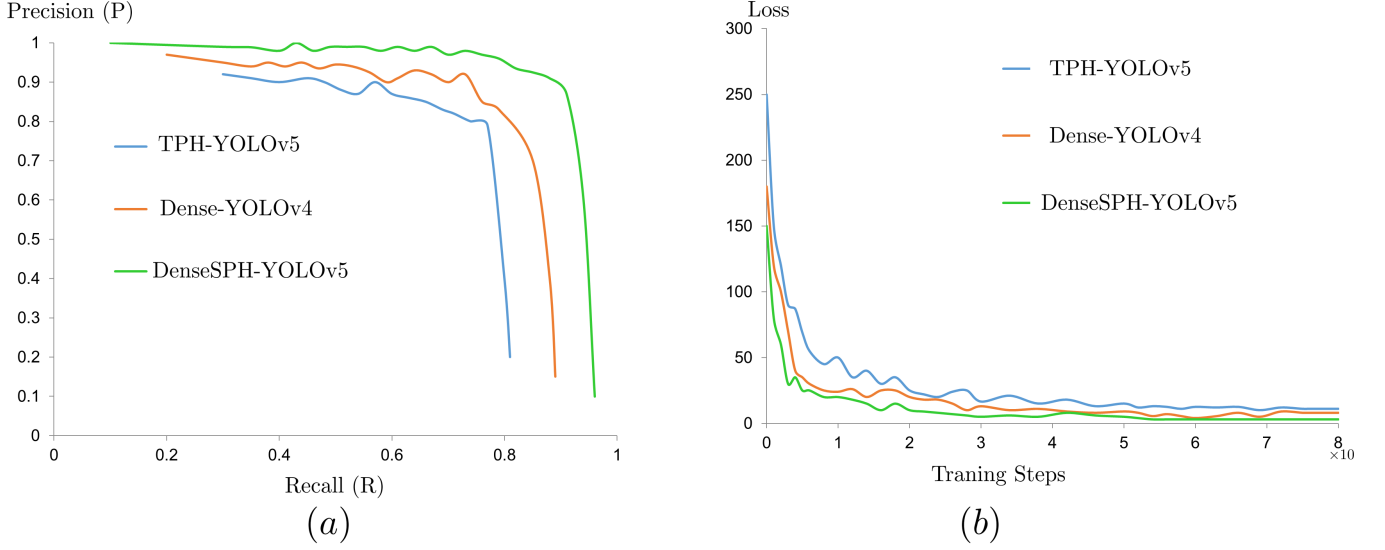


Figure 8: Comparison of (a) P-R curves; (b) loss evolution curves between TPH-YOLOv5, Dense-YOLOv4, and DenseSPH-YOLOv5.

highest F1 and mAP values of 0.811 and 0.852 which are 6.61% and 7.63% improvements over the TPH-YOLOv5, respectively. Furthermore, the detection speed of 62.4 FPS obtained from DenseSPH-YOLOv5 was found to be higher than both TPH-YOLOv5 and Dense-YOLOv4. Thus, it can provide real-time road damage detection with better accuracy compared to the other two state-of-the-art models. In addition, the comparison of P-R curves between the three models have been depicted in Fig 8-(a). From the comparison of the P-R curves, one can see that DenseSPH-YOLOv5 attains a better P value for a particular R. It achieved the highest area under the P-R curve indicating superior detection performance compared to TPH-YOLOv5 and Dense-YOLOv4. Next, we compare the loss evolution curves as shown in Fig 8-(b). In the initial phase, after exhibiting several cycles of fluctuation, the loss in the DenseSPH-YOLOv5

Table 6: Comparison of detection results for individual classes between TPH-YOLOv5, Dense-YOLOv4, and DenseSPH-YOLOv5

Model	Class →	D00	D01	D10	D11	D20	D40	D43	D44	Avg.
TPH-YOLOv5	P	0.87	0.62	0.84	0.87	0.84	0.87	0.87	0.81	0.82
	R	0.61	0.89	0.49	0.51	0.71	0.74	0.81	0.88	0.71
	F1	0.72	0.73	0.62	0.64	0.77	0.79	0.83	0.84	0.75
	mAP	0.81	0.79	0.78	0.82	0.73	0.78	0.76	0.74	0.77
Dense-YOLOv4	P	0.89	0.69	0.91	0.92	0.89	0.91	0.89	0.84	0.87
	R	0.65	0.93	0.52	0.51	0.78	0.78	0.86	0.87	0.74
	F1	0.75	0.79	0.66	0.65	0.83	0.84	0.87	0.85	0.78
	mAP	0.82	0.81	0.84	0.89	0.77	0.82	0.81	0.79	0.82
DenseSPH-YOLOv5	P	0.92	0.74	0.93	0.94	0.93	0.92	0.91	0.87	0.89
	R	0.68	0.95	0.58	0.54	0.81	0.79	0.88	0.87	0.76
	F1	0.78	0.83	0.71	0.68	0.86	0.85	0.89	0.87	0.81
	mAP	0.84	0.89	0.81	0.91	0.82	0.85	0.85	0.85	0.85

model tends to saturate after approximately 50 training steps with a final loss value of 7.18. Whereas, the other two models exhibit higher fluctuation in loss evolution and yield higher final loss value. Evidently, the proposed TPH-YOLOv5 is easier to train with faster convergence characteristics demonstrating its efficacy from the computational point of view.

To further gain insight into the performances of these models, a comparison of detection results containing P, R, mAP, and F-1 values from each individual class between TPH-YOLOv5, Dense-YOLOv4, and DenseSPH-YOLOv5 has been presented in Table 6. DenseSPH-YOLOv5 has illustrated significant improvement in P and R values for various classes, in particular, for detecting longitudinal and lateral linear cracks, alligator cracks, and potholes. Thus, DenseSPH-YOLOv5 efficiently maximizes the TP value while simultaneously reducing FP and FN values for all classes. The proposed model improves 2.01% in P and 2.11% in R compared to Dense-YOLOv4. From the overall comparison, we can conclude that DenseSPH-YOLOv5 demonstrated the best performance in detecting various damage classes outperforming the other two state-of-the-art models in terms of precision and accuracy.

4.6 Detection of various damage classes:

In this section, we have demonstrated the detection results obtained from DenseSPH-YOLOv5 for eight different damage classes and compared them with TPH-YOLOv5 and Dense-YOLOv4.

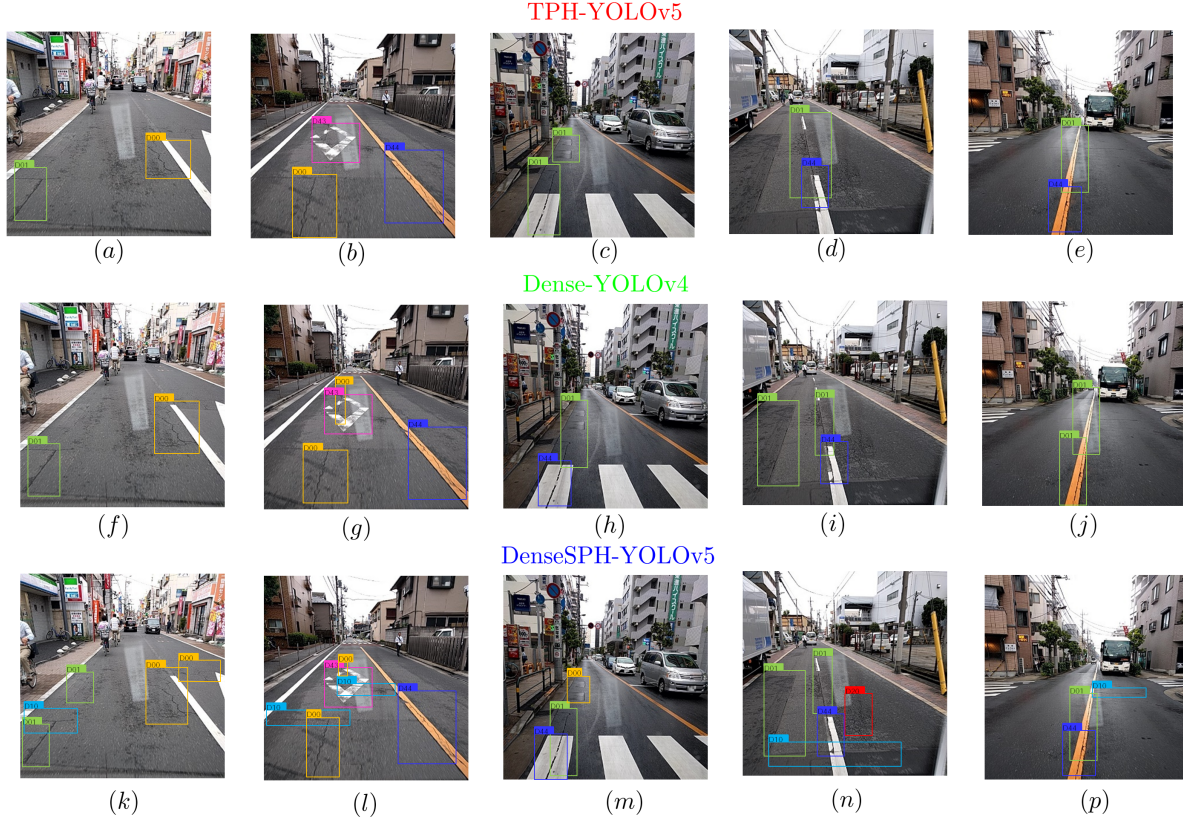


Figure 9: Comparison of various damage detection results from (a-e) TPH-YOLOv5; (f-j) Dense-YOLOv4; (k-p) DenseSPH-YOLOv5. Detailed detection results with average confidence indexes have been shown in Table 7.

Table 7: Detailed detection results from TPH-YOLOv5, Dense-YOLOv4, and DenseSPH-YOLOv5 for different damage classes as shown in Figs. 9- 10.

Figs. No	Model	Detc.	False/Undetc.	Avg. confidence Score
9 (a-e)	TPH-YOLOv5	13	8	0.71
9 (f-j)	Dense-YOLOv4	16	5	0.75
9 (k-p)	DenseSPH-YOLOv5	20	1	0.83
10 (a-e)	TPH-YOLOv5	13	7	0.67
10 (f-j)	Dense-YOLOv4	14	6	0.72
10 (k-p)	DenseSPH-YOLOv5	18	2	0.79



Figure 10: Comparison of various damage detection results from (a-e) TPH-YOLOv5; (f-j) Dense-YOLOv4; (k-p) DenseSPH-YOLOv5. Detailed detection results with average confidence scores have been shown in Table 7.

The visual representations of the detection results have been presented with confined bounding boxes with class identifiers (see Table 1) as shown in Figs. 9-10. Corresponding detailed detection results consisting of the number of detected and undetected target classes with average confidence scores have been reported in Table. 7. From the overall comparison, it can be concluded that the proposed model shows its efficacy by precisely detecting the target objects with high average confidence index values. At the same time, it minimizes the false and missed-detection results compared to both TPH-YOLOv5 and Dense-YOLOv4 models. Particularly, when the multiple target objects have a significant degree of overlap between them, the bounding box prediction from the proposed DenseSPH-YOLOv5 is quite accurate in detecting each target object as illustrated in Figs. 9-(l, n) and Figs. 10-(k, n).

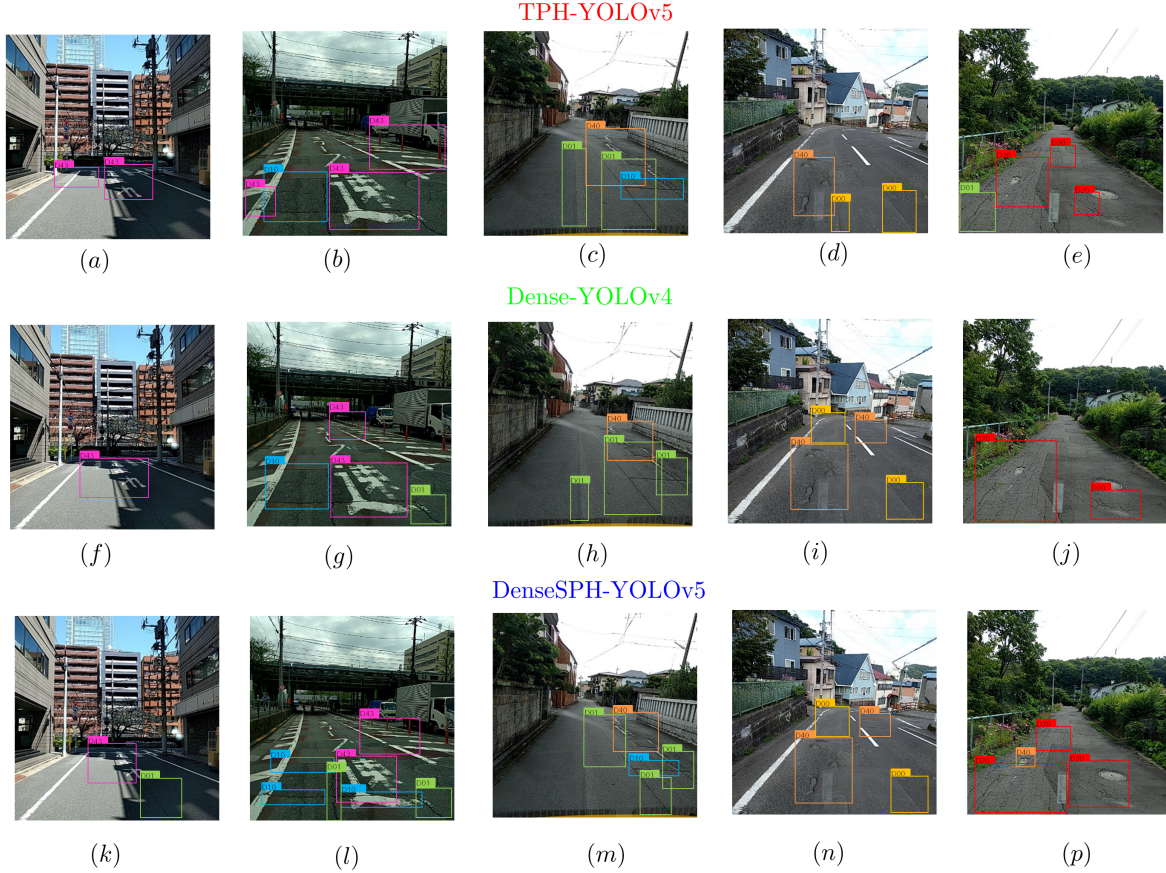


Figure 11: Comparison of damage detection results under various challenging scenarios from (a-e) TPH-YOLOv5; (f-j) Dense-YOLOv4; (k-p) DenseSPH-YOLOv5. Detailed detection results with average confidence indexes have been shown in Table 6.

4.7 Detection under challenging scenarios:

In this section, we have extended the detection under some challenging scenarios as shown in Fig. 11 to demonstrate the efficacy of the proposed DenseSPH-YOLOv5. The detailed detection results that consist of the total number of detected and undetected target classes with average confidence scores have been reported in Table. 8. Here we consider various complex backgrounds and challenging environments where the target class is predominately difficult to detect due to the presence of shadows. Additionally, there is some degree of occlusion of overlapping bounding boxes between target classes. It is a challenging task to detect target objects individually for an object detection model. Thus, superior feature extraction is critical to detect various target classes efficiently and correctly. In such cases, the proposed DenseSPH-YOLOv5 has demonstrated its superiority in terms of boundary box precision with

Table 8: Detailed detection results from TPH-YOLOv5, Dense-YOLOv4, and DenseSPH-YOLOv5 for different damage classes as shown in Fig. 11.

Figs. No	Model	Detc.	False/Undetc.	Avg. confidence Score
11 (a)-(e)	TPH-YOLOv5	13	10	0.68
11 (f)-(j)	Dense-YOLOv4	15	8	0.69
11 (k)-(p)	DenseSPH-YOLOv5	19	4	0.77

Table 9: Detection result comparison from the DenseSPH-YOLOv5 for original RGB, greyscale, low resolution, and various brightness intensity (75 % and 50 %) images as shown in Fig. 12.

Figs. No	Original		Grey scale		Low resolution		Brightness-75 %		Brightness-50 %	
	Det.	Undet.	Det.	Undet.	Det.	Undet.	Det.	Undet.	Det.	Undet.
Figs. 12-(a-e)	6	0	5	1	4	2	6	0	5	1
Figs. 12-(f-j)	3	1	4	0	2	2	3	1	3	1
Figs. 12-(k-p)	5	0	5	0	2	3	5	0	3	2

a higher average confidence score compared to the other two models. Notably, it significantly reduces the false or missed detection (10 to 4 compared to TPH-YOLOv5) and consequently, the confidence scores have been improved which is evident from Table 8. Overall, based on the detection results for the various damage classes, the proposed DenseSPH-YOLOv5 illustrates superior detection ability, in particular, in detecting the presence of shadows compared to TPH-YOLOv5 and Dense-YOLOv4 models.

4.8 Detection under Greyscale, low resolution, and different illumination intensities:

In this section, the detection accuracy of the DenseSPH-YOLOv5 has been further tested with grayscale and pixelated low-resolution (100×100) images as shown in Fig. 12. Additionally, prediction results under different illumination intensities (i.e., brightness-75% and brightness-50%) have been studied and compared with the detection result for original RGB images. In Table 9, detailed detection results with confidence scores have been reported. For grayscale images, the proposed model has demonstrated impressive performance with accurate bounding box prediction with a better bounding box confidence score as shown in Figs. 12-(b, g,

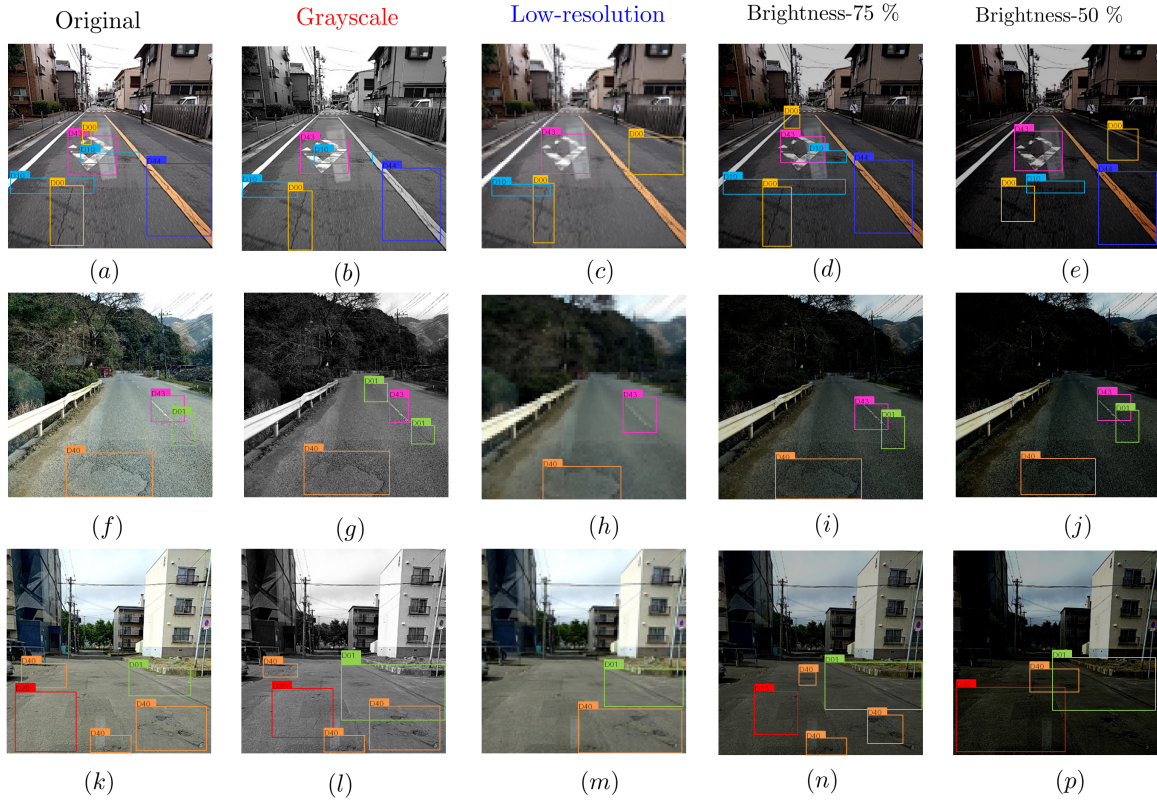


Figure 12: Detection results for (a, f, k) original RGB images; (b, g, l) corresponding grey scale images; (c, h, m) low resolution images; (d, i, n) 75 % brightness intensity; (e, j, p) 50 % brightness intensity from the DenseSPH-YOLOv5. Detailed detection results have been shown in Table 6.

l). For pixelated low-resolution images, the performance of DenseSPH-YOLOv5 has been slightly diminished, however, it can still detect most of the target class with reasonable accuracy. Similarly, the proposed model demonstrates superior detection results under different illumination intensities as demonstrated in Figs. 12-(d, i, n) and Figs. 12-(e, j, p). It can be concluded from the test results that the proposed model is more adaptive in more challenging environments compared to TPH-YOLOv5 and Dense-YOLOv4 models.

5. Discussion:

From the overall detection result, it is evident that DenseSPH-YOLOv5 has higher adaptability and better capability in localizing various damage classes in a complex environment and challenging conditions compared to current state-of-the-art models. Additionally, it has demonstrated higher accuracy in bounding box detection and therefore can effectively avoid the problem of false and missed detection over other detection networks which justifies the usefulness of the proposed model in practical on-field damage detection tasks. Future work can be geared towards further optimization of detection accuracy as well as detection speed for portable on-field damage detection in a mobile computing platform. The current model can be further improved by incorporating some state-of-the-art algorithms such as YOLO-X (Ge et al., 2021), YOLOv7 (Wang et al., 2022), etc. Additionally, it can be assembled with a drone video surveillance system for real-time accurate damage detection. Furthermore, overlapping and occultation can lead to the wrong prediction which can be further improved by considering shortening the feature stride for better localization and bounding box prediction. In order to avoid overlapping boxes, it can be useful to switch from bounding boxes to points (Ribera et al., 2019) or masks (Xu et al., 2020). Moreover, one of the potential applications can be assembling object detection framework with semantic segmentation methods such as Mask R-CNN (Bharati and Pramanik, 2020), U-Net (Esser et al., 2018) to extract morphological information of various damage classes. Nonetheless, the current work elucidates the possibility of applying cutting-edge DL-based computer vision methodology for multiclass automated damage detection processes for commercial applications.

6. Conclusions :

Summarizing, in the present work, we have developed an efficient and robust object localization model DenseSPH-YOLOv5 based on an improved version of the YOLOv5 network for accurate classification and localization of damage detection. The proposed DenseSPH-YOLOv5 has been employed to detect distinct eight different road damage classes that provide superior and accurate detection under various complex and challenging environments. Evaluated on the RDD-2018 dataset, it has been found that at a detection rate of 62.40 FPS, DenseSPH-YOLOv5 has achieved mean-average precision (mAP), F1, and precision (P) values of 85.25%, 81.18%, and 89.51%, respectively outperforms existing state-of-the-art damage detection models in terms of both classification accuracy and localized bounding box prediction in detecting all damage classes. The present work effectively addresses the shortcoming of existing DL-based damage detection models and illustrates its superior potential in real-time in-field applications. In short, current work constitutes a step toward a fully automated and efficient DL-based computer vision methodology for multi-class damage detection processes.

Acknowledgements: The support of the Aeronautical Research and Development Board (Grant No. DARO/08/1051450/M/I) is gratefully acknowledged.

Conflict of interest: The authors declare that they have no known competing financial interests or personal relationships that could have appeared to influence the work reported in this paper.

References

- Agarwal, S. and Singh, D. (2015). An adaptive statistical approach for non-destructive underline crack detection of ceramic tiles using millimeter wave imaging radar for industrial application. *IEEE Sensors Journal*, 15(12):7036–7044.
- Alfarrarjeh, A., Trivedi, D., Kim, S. H., and Shahabi, C. (2018). A deep learning approach for road damage detection from smartphone images. In *2018 IEEE International Conference on Big Data (Big Data)*, pages 5201–5204. IEEE.
- Anand, S., Gupta, S., Darbari, V., and Kohli, S. (2018). Crack-pot: Autonomous road crack and pothole detection. In *2018 Digital Image Computing: Techniques and Applications (DICTA)*, pages 1–6. IEEE.
- Angulo, A., Vega-Fernández, J. A., Aguilar-Lobo, L. M., Natraj, S., and Ochoa-Ruiz, G. (2019). Road damage detection acquisition system based on deep neural networks for physical asset management. In *Mexican International Conference on Artificial Intelligence*, pages 3–14. Springer.
- Anitha, M., Hemalatha, R., and Radha, S. (2021). A survey on crack detection algorithms for concrete structures. *Advances in Smart System Technologies*, pages 639–654.
- Arya, D., Maeda, H., Ghosh, S. K., Toshniwal, D., Mraz, A., Kashiyaama, T., and Sekimoto, Y. (2021a). Deep learning-based road damage detection and classification for multiple countries. *Automation in Construction*, 132:103935.
- Arya, D., Maeda, H., Ghosh, S. K., Toshniwal, D., Omata, H., Kashiyaama, T., and Sekimoto, Y. (2020). Global road damage detection: State-of-the-art solutions. In *2020 IEEE International Conference on Big Data (Big Data)*, pages 5533–5539. IEEE.
- Arya, D., Maeda, H., Ghosh, S. K., Toshniwal, D., and Sekimoto, Y. (2021b). Rdd2020: An annotated image dataset for automatic road damage detection using deep learning. *Data in brief*, 36:107133.
- Azimi, M., Eslamlou, A. D., and Pekcan, G. (2020). Data-driven structural health monitoring and damage detection through deep learning: State-of-the-art review. *Sensors*, 20(10):2778.

- Bang, S., Park, S., Kim, H., Yoon, Y., and Kim, H. (2018). A deep residual network with transfer learning for pixel-level road crack detection. *Network*, 93(84.90):89--03.
- Bharati, P. and Pramanik, A. (2020). Deep learning techniques—r-cnn to mask r-cnn: a survey. *Computational Intelligence in Pattern Recognition*, pages 657--668.
- Biçici, S. and Zeybek, M. (2021). An approach for the automated extraction of road surface distress from a uav-derived point cloud. *Automation in Construction*, 122:103475.
- Bochkovskiy, A., Wang, C.-Y., and Liao, H.-Y. M. (2020). Yolov4: Optimal speed and accuracy of object detection.
- Bose, R. and Roy, A. (2022). Accurate deep learning sub-grid scale models for large eddy simulations. *Bulletin of the American Physical Society*.
- Cao, M.-T., Tran, Q.-V., Nguyen, N.-M., and Chang, K.-T. (2020). Survey on performance of deep learning models for detecting road damages using multiple dashcam image resources. *Advanced Engineering Informatics*, 46:101182.
- Chandio, A., Gui, G., Kumar, T., Ullah, I., Ranjbarzadeh, R., Roy, A. M., Hussain, A., and Shen, Y. (2022). Precise single-stage detector. *arXiv preprint arXiv:2210.04252*.
- Chen, J. and Cho, Y. K. (2022). Crackembed: Point feature embedding for crack segmentation from disaster site point clouds with anomaly detection. *Advanced Engineering Informatics*, 52:101550.
- Chen, Q., Huang, Y., Sun, H., and Huang, W. (2021). Pavement crack detection using hessian structure propagation. *Advanced Engineering Informatics*, 49:101303.
- Chow, J. K., Su, Z., Wu, J., Tan, P. S., Mao, X., and Wang, Y.-H. (2020). Anomaly detection of defects on concrete structures with the convolutional autoencoder. *Advanced Engineering Informatics*, 45:101105.
- Davis, J. and Goadrich, M. (2006). The relationship between precision-recall and roc curves. In *Proceedings of the 23rd international conference on Machine learning*, pages 233--240.

- Dong, J., Meng, W., Liu, Y., and Ti, J. (2021). A framework of pavement management system based on iot and big data. *Advanced Engineering Informatics*, 47:101226.
- Dorafshan, S., Thomas, R. J., and Maguire, M. (2018). Sdnet2018: An annotated image dataset for non-contact concrete crack detection using deep convolutional neural networks. *Data in brief*, 21:1664--1668.
- Dosovitskiy, A., Beyer, L., Kolesnikov, A., Weissenborn, D., Zhai, X., Unterthiner, T., Dehghani, M., Minderer, M., Heigold, G., Gelly, S., et al. (2020). An image is worth 16x16 words: Transformers for image recognition at scale. *arXiv preprint arXiv:2010.11929*.
- Du, Y., Pan, N., Xu, Z., Deng, F., Shen, Y., and Kang, H. (2021). Pavement distress detection and classification based on yolo network. *International Journal of Pavement Engineering*, 22(13):1659--1672.
- Eisenbach, M., Stricker, R., Seichter, D., Amende, K., Debes, K., Sesselmann, M., Ebersbach, D., Stoeckert, U., and Gross, H.-M. (2017). How to get pavement distress detection ready for deep learning? a systematic approach. In *2017 international joint conference on neural networks (IJCNN)*, pages 2039--2047. IEEE.
- Esser, P., Sutter, E., and Ommer, B. (2018). A variational u-net for conditional appearance and shape generation. In *Proceedings of the IEEE conference on computer vision and pattern recognition*, pages 8857--8866.
- Fan, Z., Wu, Y., Lu, J., and Li, W. (2018). Automatic pavement crack detection based on structured prediction with the convolutional neural network. *arXiv preprint arXiv:1802.02208*.
- Fang, F., Li, L., Gu, Y., Zhu, H., and Lim, J.-H. (2020). A novel hybrid approach for crack detection. *Pattern Recognition*, 107:107474.
- Ferri, C., Hernández-Orallo, J., and Modroi, R. (2009). An experimental comparison of performance measures for classification. *Pattern recognition letters*, 30(1):27--38.
- Ge, Z., Liu, S., Wang, F., Li, Z., and Sun, J. (2021). YOLOX: Exceeding yolo series in 2021. *arXiv preprint arXiv:2107.08430*.

- Girshick, R. (2015). Fast r-cnn in proceedings of the iee international conference on computer vision (pp. 1440--1448). *Piscataway, NJ: IEEE.[Google Scholar]*.
- Gong, H., Mu, T., Li, Q., Dai, H., Li, C., He, Z., Wang, W., Han, F., Tuniyazi, A., Li, H., et al. (2022). Swin-transformer-enabled yolov5 with attention mechanism for small object detection on satellite images. *Remote Sensing*, 14(12):2861.
- Gopalakrishnan, K. (2018). Deep learning in data-driven pavement image analysis and automated distress detection: A review. *Data*, 3(3):28.
- Gopalakrishnan, K., Khaitan, S. K., Choudhary, A., and Agrawal, A. (2017). Deep convolutional neural networks with transfer learning for computer vision-based data-driven pavement distress detection. *Construction and building materials*, 157:322--330.
- Guan, J., Yang, X., Ding, L., Cheng, X., Lee, V. C., and Jin, C. (2021). Automated pixel-level pavement distress detection based on stereo vision and deep learning. *Automation in Construction*, 129:103788.
- Guo, G. and Zhang, Z. (2022). Road damage detection algorithm for improved yolov5. *Scientific reports*, 12(1):1--12.
- Haciefendioğlu, K. and Başağa, H. B. (2022). Concrete road crack detection using deep learning-based faster r-cnn method. *Iranian Journal of Science and Technology, Transactions of Civil Engineering*, 46(2):1621--1633.
- Han, J., Zhang, D., Cheng, G., Liu, N., and Xu, D. (2018). Advanced deep-learning techniques for salient and category-specific object detection: a survey. *IEEE Signal Processing Magazine*, 35(1):84--100.
- Hanzaei, S. H., Afshar, A., and Barazandeh, F. (2017). Automatic detection and classification of the ceramic tiles' surface defects. *Pattern Recognition*, 66:174--189.
- Hartmann, T. and Trappey, A. (2020). Advanced engineering informatics-philosophical and methodological foundations with examples from civil and construction engineering. *Developments in the built environment*, 4:100020.

- He, K., Gkioxari, G., Dollár, P., and Girshick, R. (2017). Mask r-cnn. in proceedings of the iee international conference on computer vision.
- He, K., Zhang, X., Ren, S., and Sun, J. (2015). Spatial pyramid pooling in deep convolutional networks for visual recognition. *IEEE transactions on pattern analysis and machine intelligence*, 37(9):1904--1916.
- Hendrycks, D. and Gimpel, K. (2016). Gaussian error linear units (gelus). *arXiv preprint arXiv:1606.08415*.
- Huang, G., Liu, Z., Van Der Maaten, L., and Weinberger, K. Q. (2017). Densely connected convolutional networks. In *Proceedings of the IEEE conference on computer vision and pattern recognition*, pages 4700--4708.
- Jamil, S., Abbas, M. S., and Roy, A. M. (2022). Distinguishing malicious drones using vision transformer. *AI*, 3(2):260--273.
- Jamil, S. and Roy, A. M. (2022). Robust pcg-based vhd detection model using d-cnns, nature-inspired algorithms, and vision transformer. *Available at SSRN: <http://dx.doi.org/10.2139/ssrn.4316752>*, page 41.
- Jamil, S. and Roy, A. M. (2023). An efficient and robust phonocardiography (pcg)-based valvular heart diseases (vhd) detection framework using vision transformer (vit). *Computers in Biology and Medicine*, page 106734.
- Jocher, G., Stoken, A., Borovec, J., Chaurasia, A., Changyu, L., Laughing, A., Hogan, A., Hajek, J., Diaconu, L., Marc, Y., et al. (2021). ultralytics/yolov5: v5. 0-yolov5-p6 1280 models aws supervise. ly and youtube integrations. *Zenodo*, 11.
- Kapela, R., Śniatała, P., Turkot, A., Rybarczyk, A., Pożarycki, A., Rydzewski, P., Wyczałek, M., and Bloch, A. (2015). Asphalt surfaced pavement cracks detection based on histograms of oriented gradients. In *2015 22nd International Conference Mixed Design of Integrated Circuits & Systems (MIXDES)*, pages 579--584. IEEE.
- Karaaslan, E., Bagci, U., and Catbas, F. N. (2021). Attention-guided analysis of infrastructure damage with semi-supervised deep learning. *Automation in Construction*, 125:103634.

- Khan, W., Kumar, T., Cheng, Z., Raj, K., Roy, A. M., and Luo, B. (2022a). Sql and nosql databases software architectures performance analysis and assessments--a systematic literature review. *arXiv preprint arXiv:2209.06977*.
- Khan, W., Raj, K., Kumar, T., Roy, A. M., and Luo, B. (2022b). Introducing urdu digits dataset with demonstration of an efficient and robust noisy decoder-based pseudo example generator. *Symmetry*, 14(10):1976.
- Kluger, F., Reinders, C., Raetz, K., Schelske, P., Wandt, B., Ackermann, H., and Rosenhahn, B. (2018). Region-based cycle-consistent data augmentation for object detection. In *2018 IEEE International Conference on Big Data (Big Data)*, pages 5205--5211. IEEE.
- Koch, C., Georgieva, K., Kasireddy, V., Akinci, B., and Fieguth, P. (2015). A review on computer vision based defect detection and condition assessment of concrete and asphalt civil infrastructure. *Advanced Engineering Informatics*, 29(2):196--210.
- LeCun, Y., Bengio, Y., and Hinton, G. (2015). Deep learning. *nature*, 521(7553):436--444.
- Li, D., Xie, Q., Gong, X., Yu, Z., Xu, J., Sun, Y., and Wang, J. (2021). Automatic defect detection of metro tunnel surfaces using a vision-based inspection system. *Advanced Engineering Informatics*, 47:101206.
- Li, P., Xia, H., Zhou, B., Yan, F., and Guo, R. (2022). A method to improve the accuracy of pavement crack identification by combining a semantic segmentation and edge detection model. *Applied Sciences*, 12(9):4714.
- Li, S. and Zhao, X. (2021). Pixel-level detection and measurement of concrete crack using faster region-based convolutional neural network and morphological feature extraction. *Measurement Science and Technology*, 32(6):065010.
- Li, Y., Li, H., and Wang, H. (2018). Pixel-wise crack detection using deep local pattern predictor for robot application. *Sensors*, 18(9):3042.
- Lin, T.-Y., Goyal, P., Girshick, R., He, K., and Dollár, P. (2017a). Focal loss for dense object detection. In *Proceedings of the IEEE international conference on computer vision*, pages 2980--2988.

- Lin, T.-Y., Goyal, P., Girshick, R., He, K., and Dollár, P. (2017b). Focal loss for dense object detection. In *Proceedings of the IEEE international conference on computer vision*, pages 2980--2988.
- Lin, T.-Y., Maire, M., Belongie, S., Hays, J., Perona, P., Ramanan, D., Dollár, P., and Zitnick, C. L. (2014). Microsoft coco: Common objects in context. In *European conference on computer vision*, pages 740--755. Springer.
- Liu, S., Qi, L., Qin, H., Shi, J., and Jia, J. (2018). Path aggregation network for instance segmentation. In *Proceedings of the IEEE conference on computer vision and pattern recognition*, pages 8759--8768.
- Liu, W., Anguelov, D., Erhan, D., Szegedy, C., Reed, S., Fu, C., and Berg, A. (2016). Ssd: Single shot multibox detector,|| in european conference on computer vision (eccv).
- Liu, Z., Lin, Y., Cao, Y., Hu, H., Wei, Y., Zhang, Z., Lin, S., and Guo, B. (2021). Swin transformer: Hierarchical vision transformer using shifted windows. In *Proceedings of the IEEE/CVF International Conference on Computer Vision*, pages 10012--10022.
- Maeda, H., Kashiya, T., Sekimoto, Y., Seto, T., and Omata, H. (2021). Generative adversarial network for road damage detection. *Computer-Aided Civil and Infrastructure Engineering*, 36(1):47--60.
- Maeda, H., Sekimoto, Y., Seto, T., Kashiya, T., and Omata, H. (2018). Road damage detection and classification using deep neural networks with smartphone images. *Computer-Aided Civil and Infrastructure Engineering*, 33(12):1127--1141.
- Majidifard, H., Jin, P., Adu-Gyamfi, Y., and Buttlar, W. G. (2020). Pavement image datasets: A new benchmark dataset to classify and densify pavement distresses. *Transportation Research Record*, 2674(2):328--339.
- Mandal, V., Mussah, A. R., and Adu-Gyamfi, Y. (2020). Deep learning frameworks for pavement distress classification: A comparative analysis. In *2020 IEEE International Conference on Big Data (Big Data)*, pages 5577--5583. IEEE.
- Misra, D. (2020). Mish: A self regularized non-monotonic activation function.

- Mohan, A. and Poobal, S. (2018). Crack detection using image processing: A critical review and analysis. *Alexandria Engineering Journal*, 57(2):787--798.
- Naddaf-Sh, S., Naddaf-Sh, M.-M., Kashani, A. R., and Zargarzadeh, H. (2020). An efficient and scalable deep learning approach for road damage detection. In *2020 IEEE International Conference on Big Data (Big Data)*, pages 5602--5608. IEEE.
- Nath, N. D., Cheng, C.-S., and Behzadan, A. H. (2022). Drone mapping of damage information in gps-denied disaster sites. *Advanced Engineering Informatics*, 51:101450.
- Nhat-Duc, H., Nguyen, Q.-L., and Tran, V.-D. (2018). Automatic recognition of asphalt pavement cracks using metaheuristic optimized edge detection algorithms and convolution neural network. *Automation in Construction*, 94:203--213.
- Ni, F., He, Z., Jiang, S., Wang, W., and Zhang, J. (2022). A generative adversarial learning strategy for enhanced lightweight crack delineation networks. *Advanced Engineering Informatics*, 52:101575.
- Oliveira, H. and Correia, P. L. (2009). Automatic road crack segmentation using entropy and image dynamic thresholding. In *2009 17th European Signal Processing Conference*, pages 622--626. IEEE.
- Patra, S., Middy, A. I., and Roy, S. (2021). Potspot: Participatory sensing based monitoring system for pothole detection using deep learning. *Multimedia Tools and Applications*, 80(16):25171--25195.
- Quintana, M., Torres, J., and Menéndez, J. M. (2015). A simplified computer vision system for road surface inspection and maintenance. *IEEE Transactions on Intelligent Transportation Systems*, 17(3):608--619.
- Rawat, W. and Wang, Z. (2017). Deep convolutional neural networks for image classification: A comprehensive review. *Neural computation*, 29(9):2352--2449.
- Redmon, J., Divvala, S., Girshick, R., and Farhadi, A. (2016). You only look once: Unified, real-time object detection. In *Proceedings of the IEEE conference on computer vision and pattern recognition*, pages 779--788.

- Redmon, J. and Farhadi, A. (2017). Yolo9000: better, faster, stronger. In *Proceedings of the IEEE conference on computer vision and pattern recognition*, pages 7263--7271.
- Redmon, J. and Farhadi, A. (2018). Yolov3: An incremental improvement.
- Ren, S., He, K., Girshick, R., and Sun, J. (2016). Faster r-cnn: towards real-time object detection with region proposal networks. *IEEE transactions on pattern analysis and machine intelligence*, 39(6):1137--1149.
- Rezatofghi, H., Tsoi, N., Gwak, J., Sadeghian, A., Reid, I., and Savarese, S. (2019). Generalized intersection over union: A metric and a loss for bounding box regression. In *Proceedings of the IEEE/CVF Conference on Computer Vision and Pattern Recognition*, pages 658--666.
- Ribera, J., Guera, D., Chen, Y., and Delp, E. J. (2019). Locating objects without bounding boxes. In *Proceedings of the IEEE/CVF Conference on Computer Vision and Pattern Recognition*, pages 6479--6489.
- Roy, A. M. (2022a). Adaptive transfer learning-based multiscale feature fused deep convolutional neural network for eeg mi multiclassification in brain--computer interface. *Engineering Applications of Artificial Intelligence*, 116:105347.
- Roy, A. M. (2022b). An efficient multi-scale CNN model with intrinsic feature integration for motor imagery EEG subject classification in brain-machine interfaces. *Biomedical Signal Processing and Control*, 74:103496.
- Roy, A. M. (2022c). A multi-scale fusion cnn model based on adaptive transfer learning for multi-class mi-classification in bci system. *BioRxiv*.
- Roy, A. M. and Bhaduri, J. (2021). A deep learning enabled multi-class plant disease detection model based on computer vision. *AI*, 2(3):413--428.
- Roy, A. M. and Bhaduri, J. (2022). Real-time growth stage detection model for high degree of occultation using densenet-fused YOLOv4. *Computers and Electronics in Agriculture*, 193:106694.
- Roy, A. M., Bhaduri, J., Kumar, T., and Raj, K. (2022a). A computer vision-based object localization model for endangered wildlife detection. *Ecological Economics*, *Forthcoming*.

- Roy, A. M., Bhaduri, J., Kumar, T., and Raj, K. (2022b). Wildect-yolo: An efficient and robust computer vision-based accurate object localization model for automated endangered wildlife detection. *Ecological Informatics*, page 101919.
- Roy, A. M. and Bose, R. (2023a). Deep learning-accelerated computational framework based on physics informed neural network for solution of linear elasticity. *Neural Networks*, 2:2.
- Roy, A. M. and Bose, R. (2023b). Physics-aware deep learning framework for linear elasticity. *arXiv preprint arXiv:2302.09668*.
- Roy, A. M., Bose, R., and Bhaduri, J. (2022c). A fast accurate fine-grain object detection model based on YOLOv4 deep neural network. *Neural Computing and Applications*, pages 1--27.
- Roy, A. M. and Guha, S. (2022). Elastoplastic physics-informed deep learning approach for j2 plasticity. *Available at SSRN: <https://ssrn.com/abstract=4332254>*, page 48.
- Roy, A. M. and Guha, S. (2023). A data-driven physics-constrained deep learning computational framework for solving von mises plasticity. *Engineering Applications of Artificial Intelligence*, 122:106049.
- Shang, H., Sun, C., Liu, J., Chen, X., and Yan, R. (2023). Defect-aware transformer network for intelligent visual surface defect detection. *Advanced Engineering Informatics*, 55:101882.
- Silva, W. R. L. d. and Lucena, D. S. d. (2018). Concrete cracks detection based on deep learning image classification. In *Proceedings*, volume 2, page 489. MDPI AG.
- Singh, A., Raj, K., Kumar, T., Verma, S., and Roy, A. M. (2023a). Deep learning-based cost-effective and responsive robot for autism treatment. *Drones*, 7(2):81.
- Singh, A., Ranjbarzadeh, R., Raj, K., Kumar, T., and Roy, A. M. (2023b). Understanding eeg signals for subject-wise definition of armoni activities. *arXiv preprint arXiv:2301.00948*.
- Stricker, R., Eisenbach, M., Sesselmann, M., Debes, K., and Gross, H.-M. (2019). Improving visual road condition assessment by extensive experiments on the extended gaps dataset. In *2019 International Joint Conference on Neural Networks (IJCNN)*, pages 1--8. IEEE.

- Varadharajan, S., Jose, S., Sharma, K., Wander, L., and Mertz, C. (2014). Vision for road inspection. In *IEEE winter conference on applications of computer vision*, pages 115--122. IEEE.
- Vaswani, A., Shazeer, N., Parmar, N., Uszkoreit, J., Jones, L., Gomez, A. N., Kaiser, L., and Polosukhin, I. (2017). Attention is all you need. *Advances in neural information processing systems*, 30.
- Voulodimos, A., Doulamis, N., Doulamis, A., and Protopapadakis, E. (2018). Deep learning for computer vision: A brief review. *Computational intelligence and neuroscience*, 2018.
- Wang, C.-Y., Bochkovskiy, A., and Liao, H.-Y. M. (2021a). Scaled-yolov4: Scaling cross stage partial network. In *Proceedings of the IEEE/cvf conference on computer vision and pattern recognition*, pages 13029--13038.
- Wang, C.-Y., Bochkovskiy, A., and Liao, H.-Y. M. (2022). Yolov7: Trainable bag-of-freebies sets new state-of-the-art for real-time object detectors. *arXiv preprint arXiv:2207.02696*.
- Wang, C.-Y., Liao, H.-Y. M., Wu, Y.-H., Chen, P.-Y., Hsieh, J.-W., and Yeh, I.-H. (2020). Cspnet: A new backbone that can enhance learning capability of cnn. In *Proceedings of the IEEE/CVF conference on computer vision and pattern recognition workshops*, pages 390--391.
- Wang, W., Li, L., and Han, Y. (2021b). Crack detection in shadowed images on gray level deviations in a moving window and distance deviations between connected components. *Construction and Building Materials*, 271:121885.
- Wang, W., Wu, B., Yang, S., and Wang, Z. (2018a). Road damage detection and classification with faster r-cnn. In *2018 IEEE international conference on big data (Big data)*, pages 5220--5223. IEEE.
- Wang, Y. J., Ding, M., Kan, S., Zhang, S., and Lu, C. (2018b). Deep proposal and detection networks for road damage detection and classification. In *2018 IEEE International Conference on Big Data (Big Data)*, pages 5224--5227. IEEE.

- Woo, S., Park, J., Lee, J.-Y., and Kweon, I. S. (2018). Cbam: Convolutional block attention module. In *Proceedings of the European conference on computer vision (ECCV)*, pages 3--19.
- Xu, B., Wang, W., Falzon, G., Kwan, P., Guo, L., Chen, G., Tait, A., and Schneider, D. (2020). Automated cattle counting using mask r-cnn in quadcopter vision system. *Computers and Electronics in Agriculture*, 171:105300.
- Xu, R., Hao, R., and Huang, B. (2022). Efficient surface defect detection using self-supervised learning strategy and segmentation network. *Advanced Engineering Informatics*, 52:101566.
- Yun, S., Han, D., Oh, S. J., Chun, S., Choe, J., and Yoo, Y. (2019). Cutmix: Regularization strategy to train strong classifiers with localizable features. In *Proceedings of the IEEE/CVF international conference on computer vision*, pages 6023--6032.
- Zhang, A., Wang, K. C., Li, B., Yang, E., Dai, X., Peng, Y., Fei, Y., Liu, Y., Li, J. Q., and Chen, C. (2017a). Automated pixel-level pavement crack detection on 3d asphalt surfaces using a deep-learning network. *Computer-Aided Civil and Infrastructure Engineering*, 32(10):805--819.
- Zhang, H., Cisse, M., Dauphin, Y. N., and Lopez-Paz, D. (2017b). mixup: Beyond empirical risk minimization. *arXiv preprint arXiv:1710.09412*.
- Zhang, L., Yang, F., Zhang, Y. D., and Zhu, Y. J. (2016). Road crack detection using deep convolutional neural network. In *2016 IEEE international conference on image processing (ICIP)*, pages 3708--3712. IEEE.
- Zhao, H., Qin, G., and Wang, X. (2010). Improvement of canny algorithm based on pavement edge detection. In *2010 3rd International Congress on Image and Signal Processing*, volume 2, pages 964--967. IEEE.
- Zhao, Z.-Q., Zheng, P., Xu, S.-t., and Wu, X. (2019a). Object detection with deep learning: A review. *IEEE transactions on neural networks and learning systems*, 30(11):3212--3232.
- Zhao, Z.-Q., Zheng, P., Xu, S.-t., and Wu, X. (2019b). Object detection with deep learning: A review. *IEEE transactions on neural networks and learning systems*, 30(11):3212--3232.

- Zheng, Z., Wang, P., Liu, W., Li, J., Ye, R., and Ren, D. (2020). Distance-iou loss: Faster and better learning for bounding box regression. In *Proceedings of the AAAI Conference on Artificial Intelligence*, volume 34, pages 12993--13000.
- Zhu, X., Lyu, S., Wang, X., and Zhao, Q. (2021). Tph-yolov5: Improved yolov5 based on transformer prediction head for object detection on drone-captured scenarios. In *Proceedings of the IEEE/CVF International Conference on Computer Vision*, pages 2778--2788.